



Laporan Akhir Projek Penyelidikan Jangka Pendek

Tool Wear Measurement Using Machine Vision

**by
Assoc. Prof. Dr. Mani Maran a/l Ratnam**

2008

USM SHORT TERM GRANT

COMPREHENSIVE REPORT

Project title: Tool wear measurement using machine vision

Project leader: Dr. Mani Maran a/l Ratnam
School of Mechanical Engineering
Universiti Sains Malaysia,
Engineering Campus,
14300 Nibong Tebal,
Penang.

Duration of project: 15 Mei 2006 – 14 Mei 2008

Contents:

1. Introduction
 - 1.1 Project Description
 - 1.2 Project Activities
 - 1.3 Project Benefits
 - 1.4 Project Duration
 - 1.5 Approved Grant Amount
 - 1.6 Project Cost

2. Project Contribution/Achievement
 - 2.1 Thesis and publications
 - 2.2 Award

3. Conclusion

4. Acknowledgement

1. Introduction

1.1 Project Description

In any machining operation, tool wear changes the geometry of cutting tools and decreases the dimensional accuracy and surface finish of the product. Monitoring of tool wear is an important for enhancing productivity in machining operations. Many investigators worldwide have studied tool wear as a significant area of research.

There are two main methods of estimating tool wear: (i) Indirect method and (ii) direct method. Examples of indirect methods are acoustic emission, tool tip temperature monitoring, vibration signatures and cutting force monitoring. Such methods require sophisticated and expensive devices and instrument and are, therefore, difficult to use in the workshop environment. Direct methods include use of toolmaker's microscope and profile projector to directly measure tool wear.

Recently, vision systems are being exploited for such application mainly due to their high resolution, reliability and ease of automatic processing of data. Such systems are also being used with special lighting techniques to measure tool wear in 3-D. In spite of the large amount of work worldwide on the application of machine vision for tool wear monitoring, such system have been mostly implemented on computer-numerical-control (CNC) lathe and milling machines. This is because of the need to park and align the cutting tool precisely under the field of view of the camera for accurate wear measurement. Such requirement limits the application of such techniques only to CNC machines.

This objective of this project is to develop a tool wear measurement system using machine vision that can measure tool nose wear by automatically performing software correction of misalignment of the tool insert. The system developed was intended to be used in machine tool workshops to monitor tool wear and change the cutting tool at an optimum time, thus reducing damage to work piece.

The technique developed is able to remove the constraints of other vision based techniques developed worldwide to measure tool wear in which the systems are limited for use on CNC machines. The software correction of misalignment

proposed in this research is able to remove the constraint and permit application to conventional lathe machines.

1.2 Project Activities

The methodology in the research involves the various stages of work described below:

Stage 1: Literature study

This part of the work involves a literature study on the state-of-the art research worldwide on the application of machine vision in tool wear measurement in lathe machining operations.

Stage 2: Setup of machine vision system and calibration

In this stage of the work, machine vision system, comprising a CCD camera, frame grabber and personal computer will be set up using existing hardware (purchased in a previous IRPA funded project). Suitable tool fixtures will be developed to position the tool under the camera and introduce rotational and translational misalignment. A study will be carried out to determine the maximum resolution that can be obtained using various lenses and extension tubes.

Stage 3: Machining operations using conventional lathe

In this stage of the work, several machining operations will be carried out using different feed rates and spindle speeds. The objective of this work is to prepare the specimens for subsequent experiments.

Stage 4: Development of algorithms to measure tool wear in the presence of misalignment

This part of the work focuses on the development of algorithms (in Matlab) to measure tool wear in the presence of rotational and translational misalignment. A study will be carried out to identify suitable pre-processing stages necessary to improve accuracy of the tool wear measurement. The measurement results will be

compared with other techniques, such as toolmaker's microscope and profile projector.

Stage 5: Development of fixture to mount camera and lighting system of lathe machine

In this part of the work, suitable fixtures will be design and developed to mount the camera and lighting system onto the lathe machine for real-time measurement.

Stage 6: Real-time tool wear measurement

Real-time tool wear measurement will be attempted using the hardware and algorithms developed in this research in this stage of the work.

Stage 7: Study on effect of machining parameters on tool wear

In this final stage of work, a study will be carried out on the effect of machining parameters on tool wear. The possibility of measuring tool wear in the presence of misalignment will be demonstrated.

The various stages of the work are reported in the papers published and the theses produced from this research (in preparation). Detailed reports on these are available in the Appendix.

1.3 Project Benefits

The project benefits are as follows:

1. A new method of monitoring and measuring tool nose wear have been developed. This method can be used by tool manufacturers to assess the wear resistance of cutting tools under different machining conditions.
2. A non-contact method of measuring the roughness of the finished product has also been developed as part of the research. This method

allows operators to quickly assess the roughness of workpiece without removing it from the machine.

3. A method of assessing flank wear from the nose wear area has also been proposed. This method can be used to assess flank wear without removing the tool from the machine.

1.4 Project Duration

This project started in May 2006 and was completed in May 2006, that is, for duration of two years.

1.5 Approved Grant Amount

The total amount approved under the short-term grant for this project is RM14,034.00, which was disbursed in two installments.

1.6 Project Cost

The total amount spent for this project was RM13,469.76 with a balance of RM564.24.

2. Project Contribution/Achievement

2.1 Theses and publications

The contribution of this research in terms of theses and publications are as follows:

PhD thesis:

- 1) Thesis titled: Study on the effect of tool nose wear on the surface roughness and dimensional deviation of workpiece in finish turning using machine vision – Hamidreza H Shahabi (to be submitted in August 2008).

Journal papers:

Papers published:

1. H.H.Shahabi, M.M.Ratnam, 'On-line monitoring of tool wear in turning operation in the presence of tool misalignment', *Int J of Adv Manf Tech*, DOI 10.1007/s00170-007-1119-4, (2007).
2. H. H. Shahabi, M. M. Ratnam, 'In-cycle monitoring of tool nose wear and surface roughness of turned parts using machine vision', *Int J of Adv Manf Tech*, DOI 10.1007/s00170-008-1430-8 (2008).
3. H.H. Shahabi, T.H. Low, M.M. Ratnam, 'Notch wear detection in cutting tools using gradient approach and polynomial fitting', *Int J of Adv Manf Tech*, DOI 10.1007/s00170-008-1437-1 (2008).

Papers under review:

1. H.H. Shahabi, M.M Ratnam, 'Assessment of flank wear and nose radius wear from workpiece roughness profile in turning operation using machine vision', submitted to *Int J of Adv Manf Tech*.
2. W.K. Mook, H.H. Shahabi, M.M Ratnam, 'Measurement of nose radius wear in turning tools from a single 2-D image using machine vision', submitted to *Int J of Adv Manf Tech*.

Copies of the full papers are available in the Appendix attached to this report.

2.2 Award

A bronze medal was won for the product titled 'ToolMon: Tool wear monitoring and measurement system for lathe machine' in ITEX2007 held from 18-20 May 2007 in Kuala Lumpur. (Copy of certificate included in the Appendix).

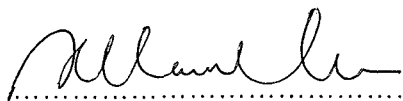
3. Conclusion

A tool wear measurement system using machine vision has been successfully developed in this research. Automatic software correction of tool misalignment allows the system to be used in-cycle in the workshop environment. Measurement can be carried out without removal of the cutting tool from the machine. The system can also be used to measure workpiece roughness without contact with the workpiece.

4. Acknowledgement

I would like to convey my sincere thanks to Universiti Sains Malaysia for the offer of the short-term grant that has enabled this research to be carried out and completed successfully.

Report prepared by:



.....
Dr. Mani Maran a/l Ratnam (Project leader)
Associate Professor,
School of Mechanical Engineering,
Engineering Campus,
Universiti Sains Malaysia,
14300 Nibong Tebal,
Penang.

Appendix

In-cycle monitoring of tool nose wear and surface roughness of turned parts using machine vision

H. H. Shahabi · M. M. Ratnam

Received: 14 June 2007 / Accepted: 4 February 2008
© Springer-Verlag London Limited 2008

Abstract Tool wear has been extensively studied in the past due to its effect on the surface quality of the finished product. Vision-based systems using a CCD camera are increasingly being used for measurement of tool wear due to their numerous advantages compared to indirect methods. Most research into tool wear monitoring using vision systems focusses on off-line measurement of wear. The effect of wear on surface roughness of the workpiece is also studied by measuring the roughness off-line using mechanical stylus methods. In this work, a vision system using a CCD camera and backlight was developed to measure the surface roughness of the turned part without removing it from the machine in-between cutting processes, i.e. in-cycle. An algorithm developed in previous work was used to automatically correct tool misalignment using the images and measure the nose wear area. The surface roughness of turned parts measured using the machine vision system was verified using the mechanical stylus method. The nose wear was measured for different feed rates and its effect on the surface roughness of the turned part was studied. The results showed that surface roughness initially decreased as the machining time of the tool increased due to increasing nose wear and then increased when notch wear occurred.

Keywords Machine vision · Tool wear · Surface roughness

1 Introduction

Tool wear and tool failure are among the limitations to unattended machining in modern manufacturing. In fact,

20% of the downtime of machine tools is reported to be due to tool failure [1]. Thus, in order to save machining costs the manufacturer has to replace worn out cutting tools 'just-in-time'. In-process (or on-line) monitoring of tool wear is therefore important in determining the best time to change the cutting tool.

Several methods of monitoring and measuring tool wear have been developed in the past. These can be broadly divided into two groups: indirect methods and direct methods. Examples of indirect methods include acoustic emission monitoring, tool-tip temperature monitoring, vibration signature analysis (acceleration signals), monitoring of motor current, and cutting force monitoring [2]. These methods normally require expensive instrumentation and are difficult to implement in a typical workshop environment. Direct methods, such as machine vision systems using a charged-couple-device (CCD) camera or optical microscope, are able to measure tool wear directly. They are simpler and require less costly equipment compared to the indirect methods. Therefore, the application of machine vision to measurement of tool wear has been of great interest in the research community in recent years [1, 3–14].

The effect of tool wear on the surface quality of machined parts is well known [13–14]. The ease of capturing and analyzing images of machined surfaces has encouraged researchers in the past to use roughness parameters for tool wear monitoring. Analysis of surface texture is one method of distinguishing a sharp tool from a worn out tool [12]. The surface roughness can also be measured directly using mechanical stylus methods. Although the stylus method is accurate it has several disadvantages. For example, the stylus and its transducer are delicate and thus the instruments must be used in a fairly vibration-free environment, and the method is slow

H. H. Shahabi · M. M. Ratnam (✉)
School of Mechanical Engineering, Engineering Campus,
Universiti Sains Malaysia,
14300 Nibong Tebal, Penang, Malaysia
e-mail: mmaran@eng.usm.my

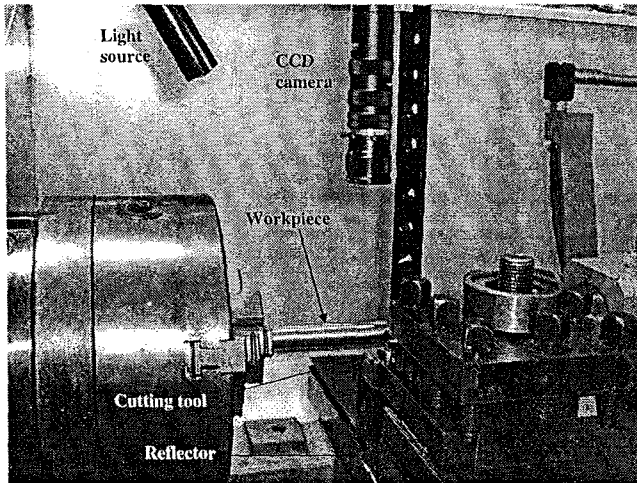


Fig. 1 System setup on lathe machine

and not suitable for in-cycle measurement of roughness in the workshop area.

In-process monitoring of surface roughness is important because the effect of tool wear on surface finish can be assessed directly. Although many optical methods for measuring tool wear and surface roughness have been proposed in the past, these methods either require the tool or the workpiece to be removed from the machine and inspected in the laboratory. In this research, a vision system

has been developed for the measurement of surface roughness of the workpiece in turning operations within the workshop area. The measurement is carried out in-between cutting processes, i.e. in-cycle, without removing either the cutting tool or workpiece from the machine.

2 System configuration

2.1 System setup

The system used for measuring the tool wear and surface roughness is shown in Fig. 1. A high-resolution (1392×1040 pixels) CCD camera (JAI CV-A1) was used to capture the images of the cutting tool and workpiece. The camera was fitted with a 50 mm lens (model GMHR35028MCN; Goyo Optical Inc., Japan) for measuring tool wear area and a 25 mm lens (model GMHR32514MCN) for measuring workpiece roughness. A 110 mm extension tube was fitted to increase the optical magnification. Backlighting was used to capture the contour of the cutting tool and workpiece. The position of the camera was adjusted so that either the cutting tool or workpiece surface could be captured. The use of the 50 mm lens resulted in a larger field-of-view due to the increase in object-to-lens distance. Since the use of a long extension tube could result in image

Fig. 2 Images of Ronchi rulings. a, b 25 mm lens. c, d 50 mm lens

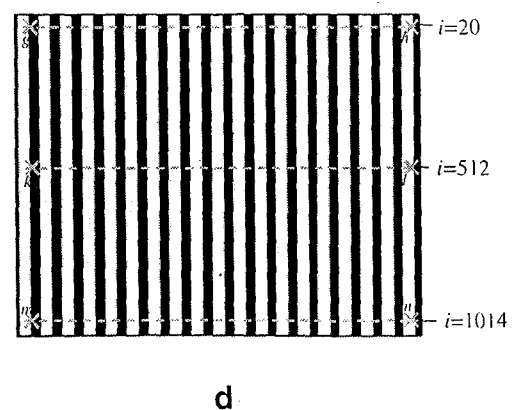
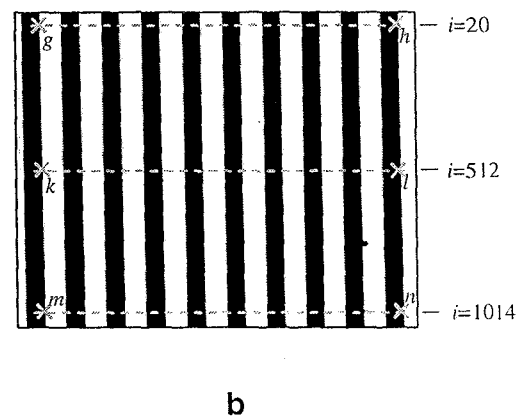
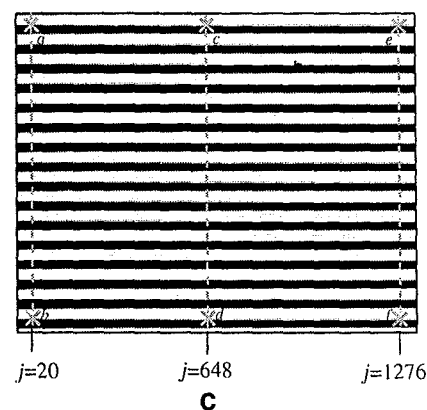
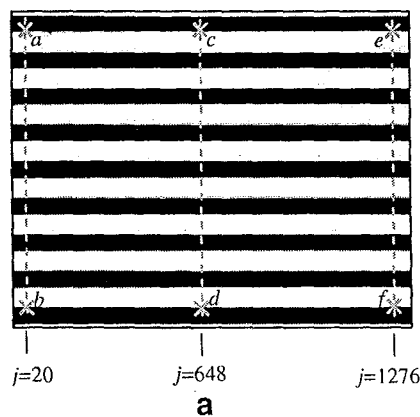


Table 1 Distances between measurement points on image (see Fig. 2) (pixels)

Points	Lens focal length	
	25 mm	50 mm
a-b	898	949
c-d	899	949
e-f	898	948
g-h	1097	1228
k-l	1098	1228
m-n	1096	1228

distortion, the presence of distortion was checked using high precision Ronchi rulings having 200 lines per inch (Edmund Optics Pte. Ltd., Singapore). Separate images of the rulings placed in horizontal and vertical positions were captured using the 25 mm and 50 mm lenses. The images were contrast enhanced and scanned at various points shown in Fig. 2a–d. The distances between these points were calculated to assess the amount of distortion. The results in Table 1 show that maximum difference in distance between the points is 2 pixels (0.18%). Since the output of the CCD camera is in pixels and the surface roughness of the workpiece must be determined in μm , it was necessary to determine the horizontal and vertical scaling factors in mm/pixel. These factors were obtained using pin gages of known dimensions and are shown in Table 2.

2.2 Machining condition

Several parameters can influence the surface roughness of the workpiece and tool wear. These include machining duration, cutting speed, feed rate, properties of cutting tool, material of workpiece, and properties of coolant. Table 3 shows the parameters used in this study.

3 Description of measurement algorithm

The various stages of the measurement of workpiece roughness are shown in Fig. 3 and are described in the

Table 2 Horizontal and vertical scale factors

Lens focal length	Direction	Scaling factor ($\mu\text{m}/\text{pixel}$)	Field of view of camera
50 mm	Horizontal	1.81	2.3 mm \times 2 mm
	Vertical	2	
25 mm	Horizontal	1	1.3 mm \times 1.1 mm
	Vertical	1.06	

Table 3 Machining parameters

Machine tool	Conventional lathe (Harrison 600; The 600 Group, UK)
Workpiece	Stainless steel rod, AISI308
Cutting tool	Uncoated cemented carbide: TPUN-16-03-04_H13A (Sandvik Co, Ltd, Sweden)
Feed rate	0.2, 0.25, 0.3, 0.4 mm/rev
Machining depth	0.5 mm
Cutting speed	58 m/min
Coolant	Air
Machining time	5, 25, 50, 75, 100, 125, 150, 175, 208 min

following sub-sections. Detailed description of the algorithm used for tool wear measurement is published separately [15].

3.1 Image acquisition

In the stage 1, a frame-grabber (DT3162; DataTranslation, Inc., USA) was used to interface the CCD camera to the computer. The frame grabber is a digitizer that acts as an image buffer. Output of the CCD camera was captured and digitized using this frame grabber.

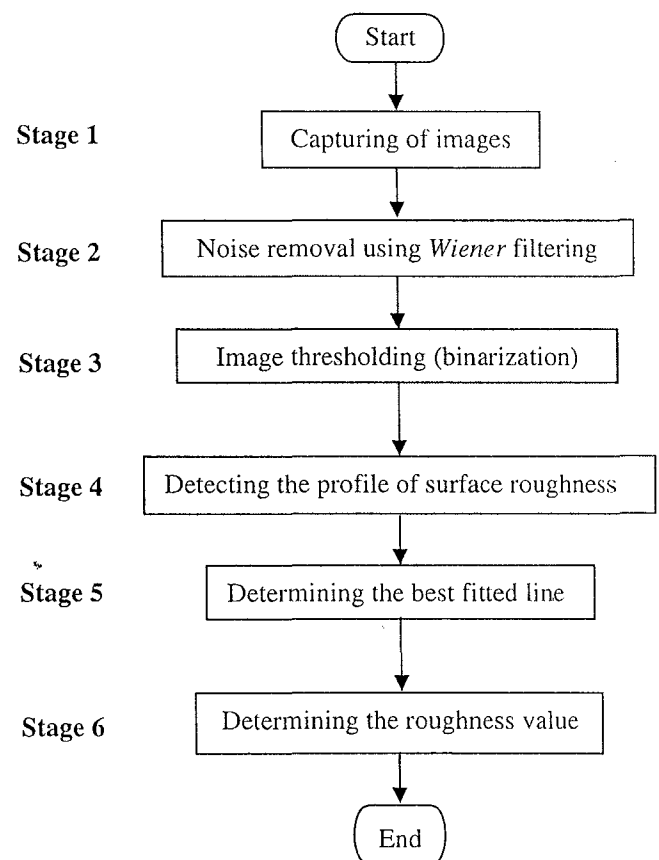
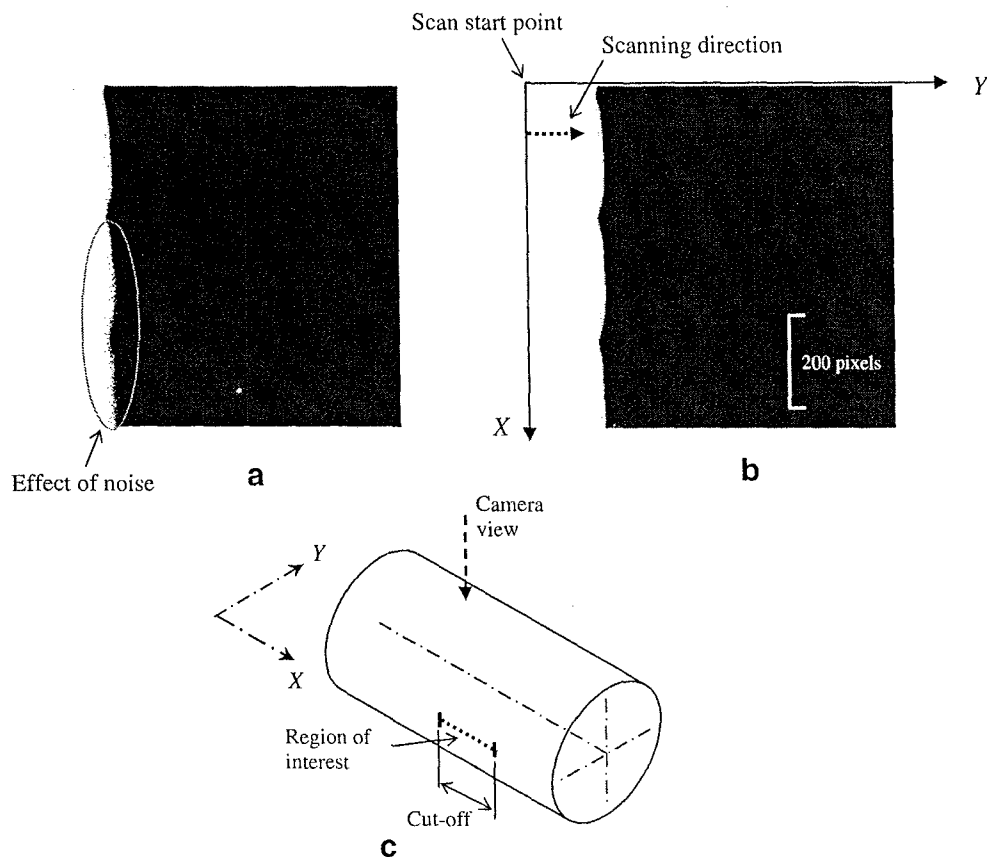
**Fig. 3** Flowchart of algorithm for roughness measurement

Fig. 4 Images of surface roughness profile. **a** Before Wiener filtering. **b** After Wiener filtering. **c** Region where surface profile is captured



3.2 Image enhancement

In stage 2, the images were enhanced using noise filtering methods. The captured image $g(x,y)$ can be represented by [16]:

$$g(x,y) = h(x,y)*f(x,y) + \eta(x,y) \tag{1}$$

where $f(x,y)$ is the original image, $h(x,y)$ is the degradation function, $\eta(x,y)$ is the additive noise term in the image and

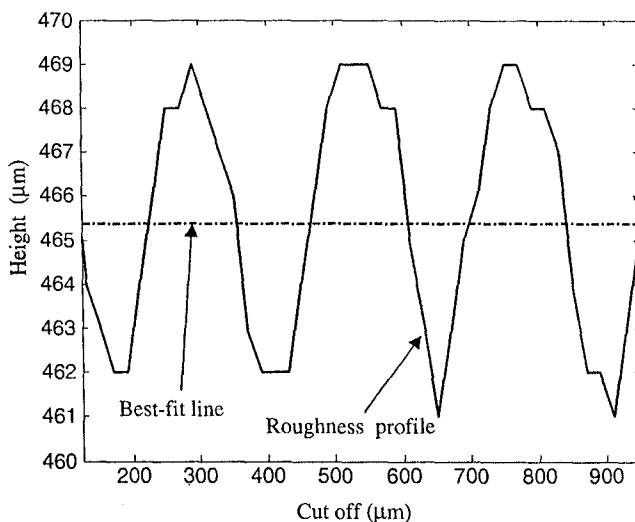


Fig. 5 Contour of roughness profile

the asterisk refers to the convolution operation. Wiener filtering was used to recover the images that were degraded by noise [16, 17]. The Wiener filtering method, introduced in 1942, is not sensitive to inverse filtering of noise and is one of the best approaches to recover images. The Wiener filter uses statistical parameters to minimize error. Although it is normally used to restore blurred images, Matlab uses this method to enhance images affected by noise using the `wiener2` command. This command does not need to have any information about the noise distribution and applies the Wiener filter adaptively using the local statistical parameters. Compared to a linear filter, the Wiener filter is more selective and preserves edges and other high frequency components in the image. Figure 4a,b shows sample images of workpiece contour before and after Wiener filtering. Figure 4c shows the view direction of the camera relative to the workpiece and the region where the roughness profile is captured.

3.3 Segmentation

In stage 3, the image was segmented to separate the workpiece (dark region) from its background (bright region) using a global thresholding method. Thresholding produces a binary image by setting all pixels in the input image for a given range of gray values to 1 and the remaining values to 0. The threshold value T is used to define

Table 4 Comparison between roughness determined using vision method and stylus method

Cutting speed (m/min)	Feed rate (mm/rev)	$R_a(v)$ μm	$R_a(s)$ μm	$\frac{ R_a(s)-R_a(v) }{R_a(s)}$ ($\times 100\%$)	$R_q(v)$ μm	$R_q(s)$ μm	$\frac{ R_q(s)-R_q(v) }{R_q(s)}$ ($\times 100\%$)
16.3	0.2	1.81	1.75	3.4%	2.14	2.10	1.9%
	0.25	2.50	2.62	4.6%	2.87	3.03	5.3%
	0.3	3.25	3.23	0.6%	3.73	3.77	1.1%
	0.4	5.23	4.95	5.7%	6.28	6.04	4.0%
23.8	0.2	1.72	1.76	2.3%	2.00	2.18	8.3%
	0.25	2.96	2.69	10.0%	3.41	3.13	9.0%
	0.3	3.38	3.49	3.2%	3.97	4.10	3.2%
	0.4	6.82	6.70	1.8%	8.02	7.78	3.1%
39.6	0.2	1.74	1.76	1.1%	2.06	2.18	5.5%
	0.25	2.58	2.67	3.4%	3.06	3.23	5.3%
	0.3	2.61	2.64	1.1%	3.11	3.15	1.3%
	0.4	6.48	6.42	0.9%	7.66	7.63	0.4%

$R_a(v)$ and $R_q(v)$: Roughness determined using vision method.
 $R_a(s)$ and $R_q(s)$: Roughness measured using stylus method.

the range of grayscale values that are set to 0 and 1. T was determined automatically using the "graythresh" command in Matlab that uses the well-known Otsu's method [18]. Otsu's algorithm uses the image histogram to determine the threshold value. The algorithm assumes that the image histogram is bimodal and determines the optimum threshold value that separates the two groups of pixels.

3.4 Roughness measurement

The captured image shows the workpiece surface contour and the roughness value can be determined directly from the image without the need of a stylus method. In stage 4, the surface contour in the binarized image was detected using an algorithm written in Matlab. Each image is read as a matrix of X and Y (row by column). Since in the binarized images, white areas have an intensity value of 1 and black

areas have an intensity value of 0, the surface profile of the workpiece is detected when the intensity value changes from 1 to 0. The algorithm starts scanning from the first pixel of the first column. If the first pixel value is 0 the scanning stops and begins at the second row. If it is not 0 it checks the second pixel in the same row. This operation continues to search for a 0 pixel in the first row. Then, the first 0 value pixel of the second row is searched. This scanning is repeated for all the rows to detect the contour of the surface roughness profile.

A typical profile is shown in Fig. 5. Since the detected roughness profile is in pixels, the scaling factors obtained earlier were used to convert the roughness to micrometers. The surface roughness can be determined by subtracting the mean value of the roughness profile from each point on the contour. In the fifth stage the best-fit line of the detected contour, considered as a mean line, was determined. The best fitted line is also shown in Fig. 5.

In stage 6, two amplitude parameters, the centerline average (R_a) and root mean square (R_q), which are the most common parameters of the roughness test, were determined. R_a and R_q are difficult to measure directly but their reliability are higher compared to other roughness parameters. If equal spaces of horizontal distances, assumed as $1,2,3,\dots,n$, have respective absolute heights $h_1, h_2, h_3, h_4, \dots, h_n$, then [19]

$$R_a = \frac{h_1 + h_2 + h_3 \dots + h_n}{n} = \frac{1}{n} \sum_{i=1}^n h_i \tag{2}$$

$$R_q = \sqrt{\frac{h_1^2 + h_2^2 + h_3^2 \dots + h_n^2}{n}} = \sqrt{\frac{\sum_{i=1}^n h_i^2}{n}} \tag{3}$$

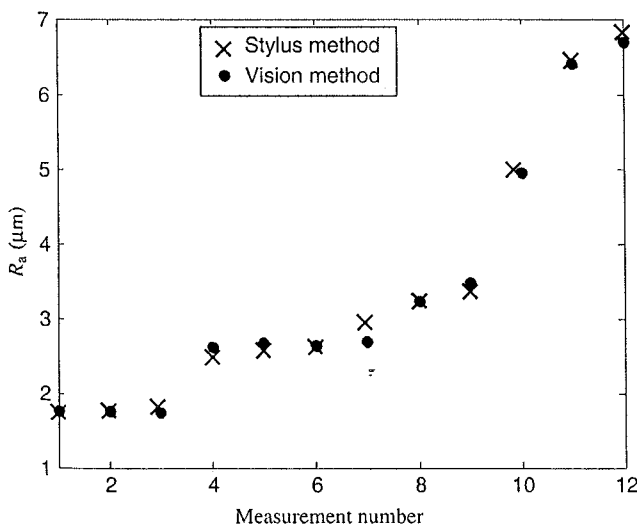
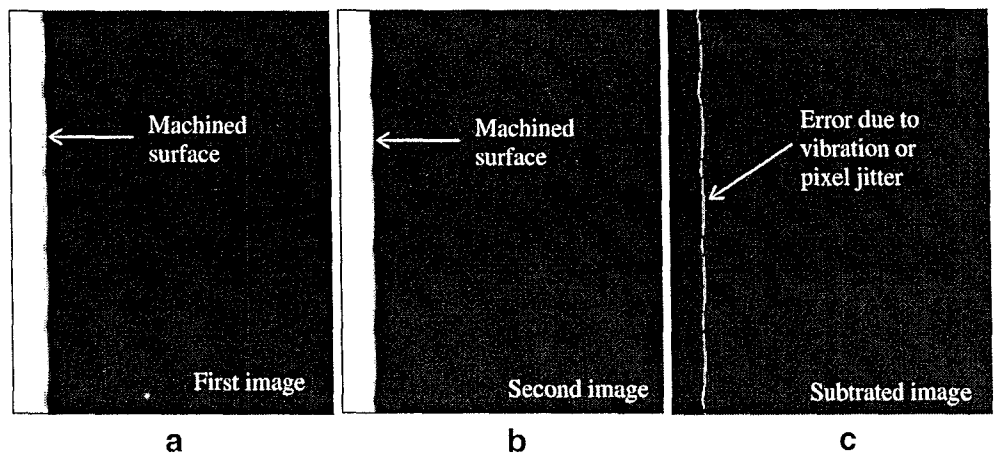


Fig. 6 Comparison between roughness determined using the vision method and the stylus method

Fig. 7 Images of surface roughness profile in the presence of ambient vibration. **a** First image. **b** Second image. **c** Subtraction of images in **a** and **b**



In this work, n is equal to the length of the image in pixels along the roughness profile.

4 Results and discussion

4.1 System verification

4.1.1 Surface roughness measurement using a CCD camera

To prepare the workpiece, an uncoated carbide insert was used to machine a stainless steel rod. The workpiece was removed from the lathe machine and 16 images of the workpiece surface contour were captured at various locations using the vision system. The average value of R_a and R_q of these 16 images were calculated from the profiles extracted using the algorithm described earlier. This was repeated for 12 different workpieces under different cutting speeds and feed rates shown in Table 4.

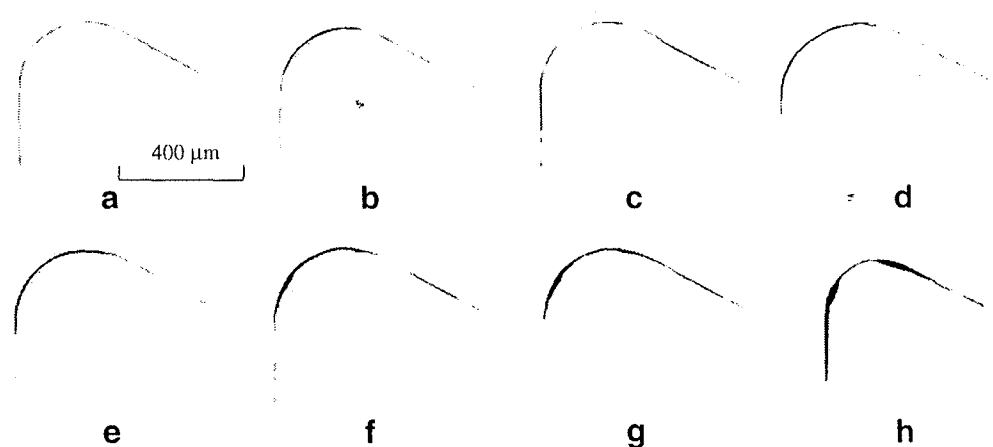
A roughness tester (model SJ-201P; Mitutoyo) was used to verify the results of roughness measured using the vision system. Each surface was measured 16 times in different regions of the workpiece. Table 4 also shows the results of

surface roughness measurement and comparison with the mechanical stylus method. The results show that the maximum deviation for R_a and R_q between vision and stylus methods are, respectively, 10% and 9%. Figure 6 show a plot of R_a versus measurement number determined using the vision method and stylus measurement. The comparison shows that the vision method is able to provide reliable roughness values.

4.1.2 Effect of ambient lighting

To study the effect of ambient lighting on the system error, 16 images of one region of a workpiece were captured under different ambient light intensities. A light meter (Lx-101A, LT Lutron) was used to record the ambient light intensity. The light intensity was varied between 12 lux and 1935 lux. The surface roughness of all 16 profiles was determined to evaluate the system error due to different ambient light intensities. The mean values of R_a and R_q for 16 images due to the different light intensities were found to be $1.81 \mu\text{m}$ and $2.20 \mu\text{m}$. The maximum deviations between the 16 values were 2.1% and 2.2% for R_a and R_q , respectively.

Fig. 8 Images of cutting tool wear area. **a** After 5 min. **b** After 25 min. **c** After 50 min. **d** After 75 min. **e** After 100 min. **f** After 125 min. **g** After 175 min. **h** After 208 min



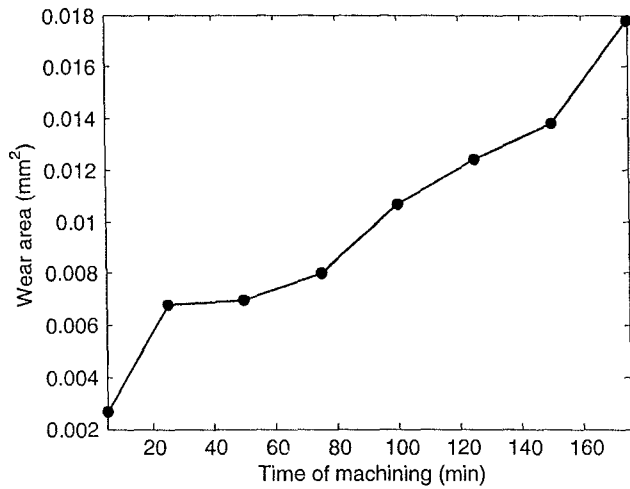


Fig. 9 Plot of cutting tool wear area vs. machining time

4.1.3 Effect of vibration

To study the effect of vibration in the environment on the measured roughness, 16 different images of one region of a workpiece were captured under the same lighting condition. Since the workpiece was not moved, any difference between images could be due to ambient vibration, changes caused by thermal effects, or pixel jitter during image capture. Since the experiment was carried out under room temperature conditions the difference is mostly likely due to vibration or pixel jitter. Figure 7a,b shows two images of the workpiece profile and Fig. 7c is their subtraction result. The white pixels in the figure after subtraction show the effect of vibration or pixel jitter. The surface roughness of 16 images of the workpiece profile was determined to investigate the effect of these errors.

The average values of R_a and R_q of the 16 images in the presence of different ambient vibration were found to be 1.84 and 2.24 μm , respectively. The deviations between the 16 values of R_a and R_q determined using the vision method are 1.99% and 0.8%, respectively. Since this deviation is

small the system can be considered as unaffected seriously by environmental disturbances.

4.2 Tool wear and its effect on surface roughness

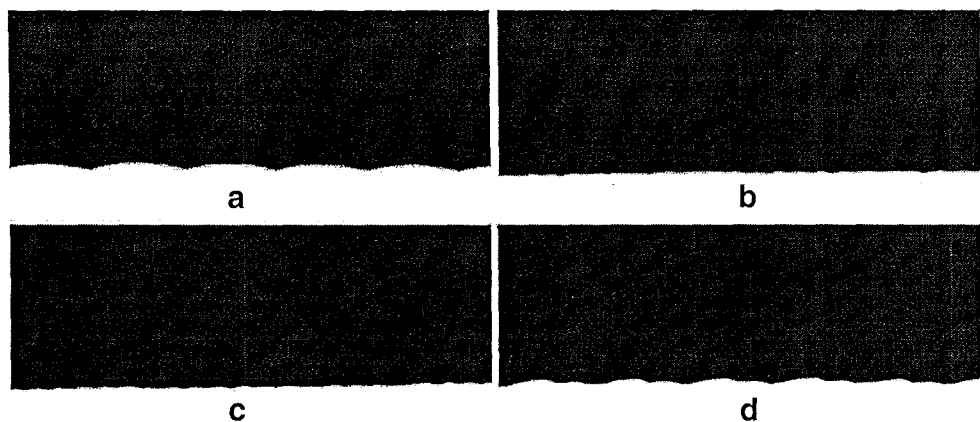
4.2.1 Tool wear measurement

The images of the cutting tool show the tool contours and from these images the area of the cutting tool tips can be determined. When the cutting tool tips are worn, the area of the tool tip decreases. By subtracting the images of worn and unworn tools the wear area can be determined. Figure 8a–h shows eight images of tool wear areas for machining time between 5 and 208 minutes. The subtraction was carried out after applying a conforming method that corrects misalignment between the images [15]. This method corrects misalignment in the cutting tool using the captured images. The wear area was determined by finding the area of the subtracted image (in pixels) and multiplying it by the horizontal and vertical scaling factors given in Table 2. Figure 9 shows a plot of wear area against machining time where the wear area increases gradually between 5 and 175 minutes.

4.2.2 Effect of tool wear on surface roughness

To study the effect of tool wear on surface roughness the workpieces were machined using the worn cutting tool. The machining parameters are given in Table 3. For each workpiece 16 images of surface roughness profiles were captured. Figure 10a–d shows the images of workpiece profiles for different machining times, and Fig. 11a–d shows the corresponding roughness plots. The images shown in Fig. 10a–d were captured from workpieces machined with feed rates of 0.2 mm/rev. The surface roughness initially decreased and then increased after a certain machining time. A study of other images captured from the workpieces prepared using feed rates of 0.25, 0.3,

Fig. 10 Images of workpiece profile. a New tool. b After 50 min. c After 75 min. d After 175 min



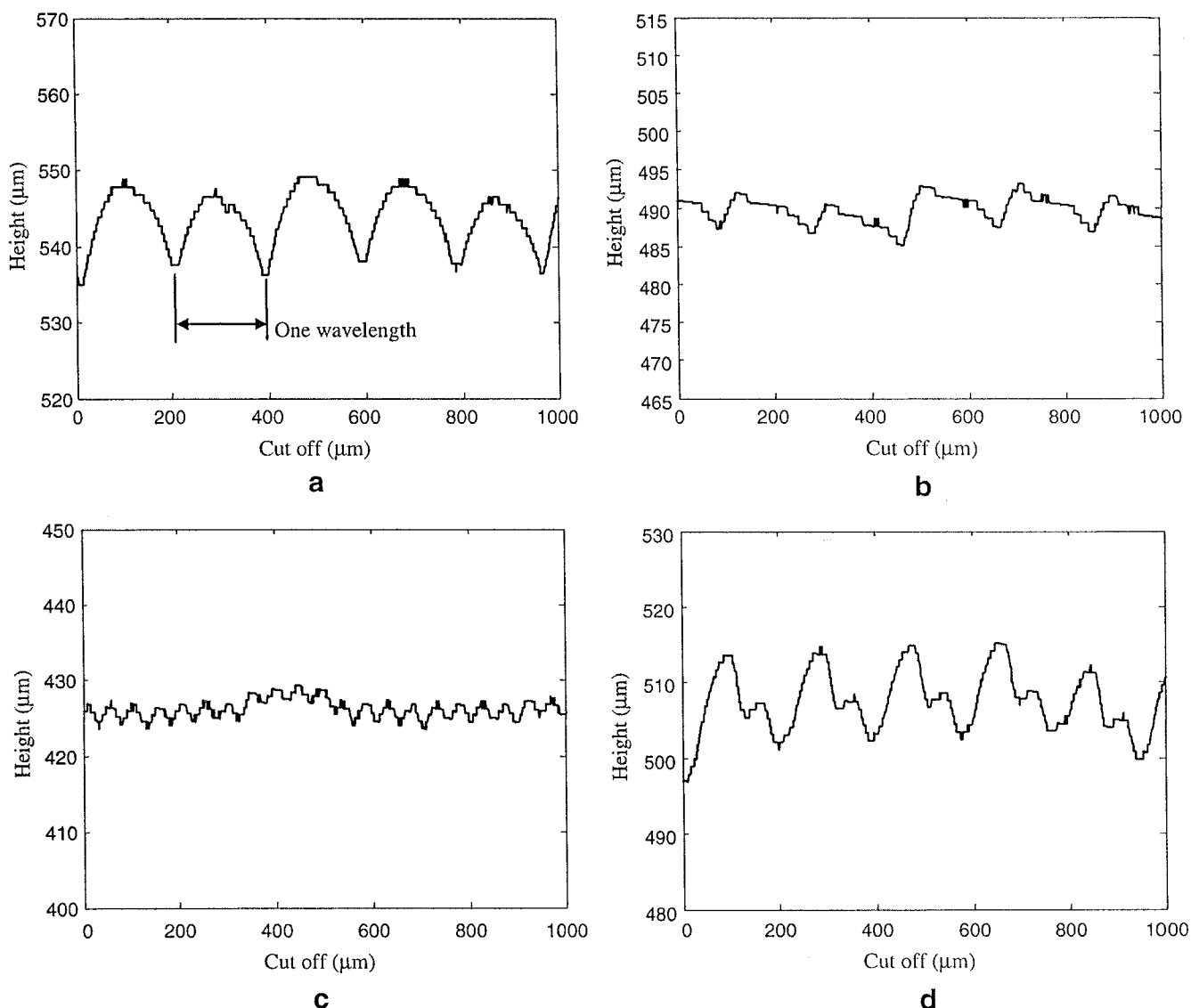


Fig. 11 Roughness profiles of workpiece. a New tool. b After 50 min. c After 75 min. d After 175 min

and 0.4 mm/rev also revealed similar trends. The reason for this can be explained by plotting the workpiece surface profiles.

As Fig. 11a–d shows, the surface profile is repeating more or less periodically as expected and horizontal length of each cycle is nearly equal to the machining feed per revolution (0.2 mm). The fluctuation in the periodic profile in some of the cases is due to disturbances in the machining process because the maximum fluctuation is less than 5 μm. The ‘period’ of each profile does not change when the machining time is increased, rather only the amplitude changes. When the cutting tool is new (sharp) the roughness is maximum and when the tool is used for some time the roughness decreases. This is due to increasing nose wear that causes a smearing effect on the workpiece. This phenomenon continues until a machining time of approximately 75 min for feed rates of 0.25 mm/rev and 0.3 mm/rev. After 100

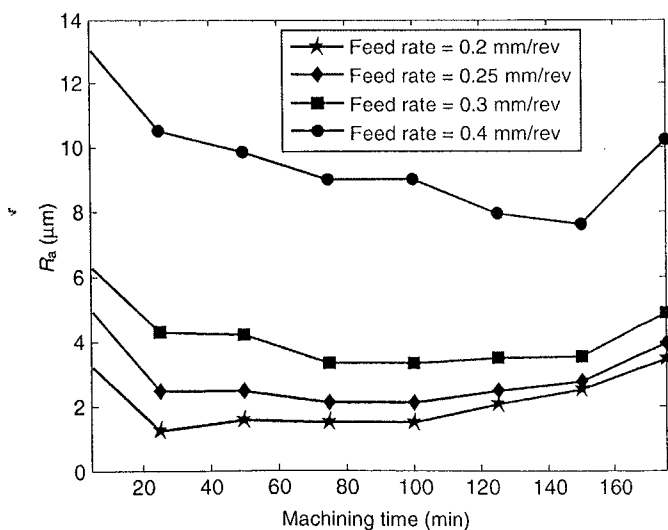


Fig. 12 Effect of feed rate and machining time on R_a

minutes of machining time the roughness increases and continues to increase until the cutting tool breaks or is badly worn (175 min). Figure 12 shows the variation of surface roughness with machining time determined using the machine vision system. When the feed rate is higher, the roughness value is greater at any machining time.

One wavelength of roughness profile for each machining time was used to study the roughness profile more closely (Fig. 13a–d). Each of the roughness profiles was plotted using the same scale in the horizontal and vertical axes. Comparison of cutting tool geometry and wavelength of roughness profile shows a close correlation between the two. The gradual growth of nose wear causes flattening of the roughness profile and therefore the surface roughness

decreases. However, the growth of notch wear causes changes to the shape of the roughness profile to a less flattened shape (Fig. 13d) and therefore the roughness increases.

In previous research, Choudhury et al. [3] reported that when flank wear increases the roughness value decreases. Kassim et al. [2] also described that the surface roughness decreases as flank wear increases if the influence of flank wear is predominant. They reported that flank wear is predominant at the initial stage of tool wear, but in the second stage other types of wear such as notch wear and crater wear have greater effects on surface roughness, though the reason for this observation was not clear. However, flank wear is not a reliable parameter when a

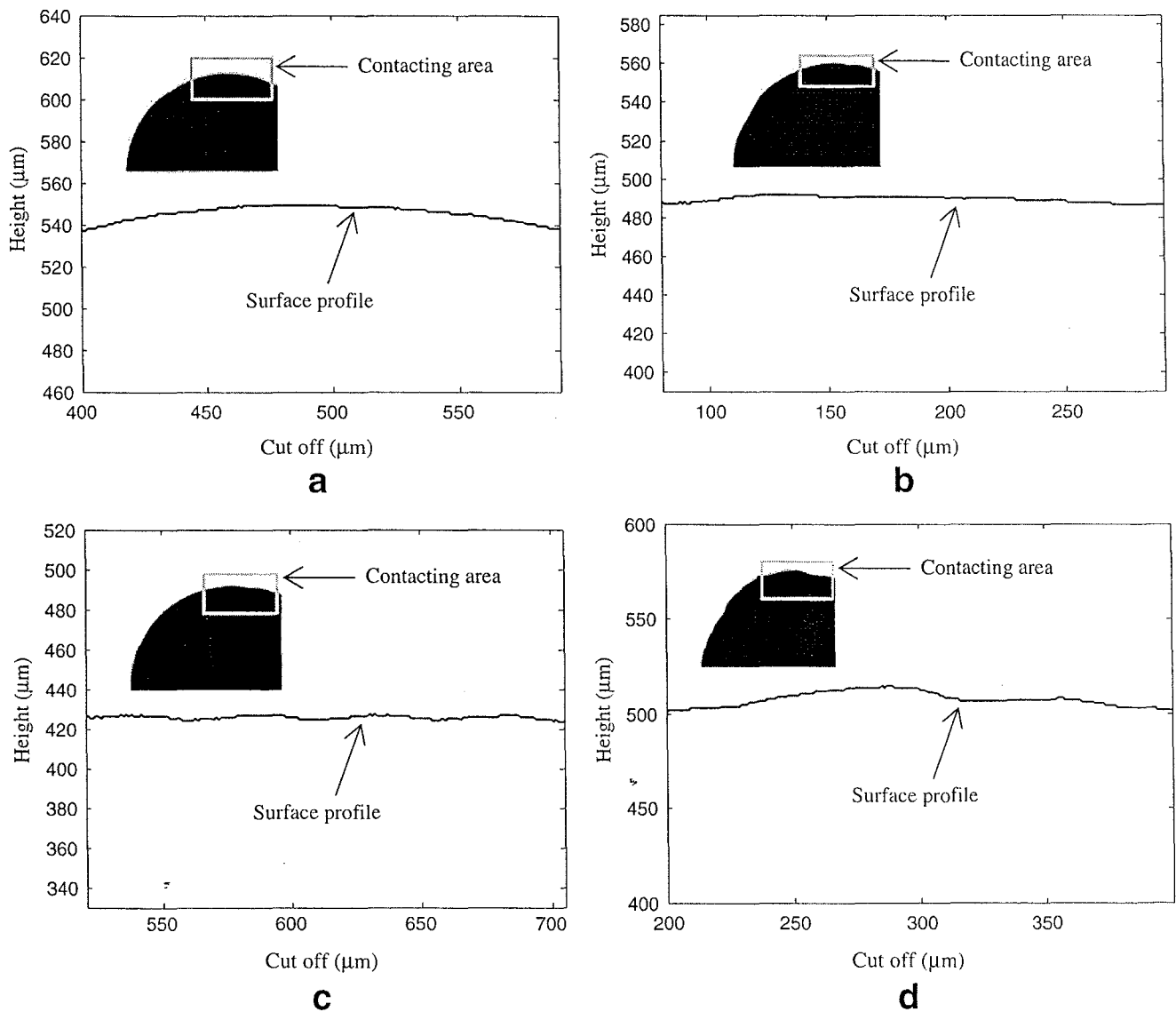


Fig. 13 Comparison between cutting tool profile and workpiece surface profiles for one wavelength. **a** New tool. **b** After 50 min. **c** After 75 min. **d** After 175 min

surface roughness requirement has to be met [19, 20]. In a similar study, Pavel et al. [13] reported that when the output of a machining process is continuous chip the roughness value increased with machining time. When the chip is not continuous the roughness value decreased with machining time. When notch wear is negligible the surface roughness decreases with flank wear, and when notch wear increases the roughness value increases. This was, however, not confirmed experimentally in their paper. The results of our study show that increasing flank wear flattens the tool nose area and this decreases the surface roughness of the workpiece. However, increasing notch wear after 75 minutes of machining time increases the roughness value. The machine vision system developed in this work can be extended to further study the effect of nose wear on workpiece surface roughness under other machining conditions, such as different workpiece materials and cutting speeds.

5 Conclusion

The noncontact method using machine vision proposed in this work and in previous work [15] enables the measurement of both cutting tool nose wear area and surface roughness of turned parts using the same setup. An algorithm that employs Wiener filtering and simple thresholding on backlit images reduces errors caused by the environmental factors such as ambient lighting and vibration. A comparative study using the stylus method of roughness measurement showed that the maximum deviation in roughness value measured using the proposed system is about 10%. A study of 2D tool wear area using the system developed shows that increasing the feed rate increases the surface roughness if other machining parameters are not changed. Also, the results show that increasing the machining time of the tool decreases the surface roughness in the first stage of machining due to increase in nose wear. However, in the second stage of machining (after 75 minutes), the roughness value increases due to the effect of growing notch wear.

The surface profiles of the workpiece show that roughness is periodic as expected, and this was clearly visible at different machining times. A close correlation was found to exist between the shape of the wear area of the cutting tool and the roughness profile. The system and measurement algorithm developed can be applied within the workshop environment for the in-cycle monitoring of tool wear and workpiece surface roughness.

Acknowledgement The authors wish to thank Universiti Sains Malaysia for the short-term grant that enabled this study to be carried out.

References

1. Kurada S, Bradley C (1997) A review of machine vision sensors for tool condition monitoring. *Comput Ind* 34:55–72
2. Kassim AA, Mian Z, Mannan MA (2004) Connectivity oriented fast Hough transform for tool wear monitoring. *Pattern Recogn* 37:1925–1933
3. Choudhury SK, Bartarya G (2003) Role of temperature and surface finish in predicting tool wear using neural network and design of experiments. *Int J Mach Tools Manuf* 43:747–753
4. Sortino M (2003) Application of statistical filtering for optical detection of tool wear. *Int J Mach Tools Manuf* 43:493–497
5. Pfeifer T, Wieggers L (2000) Reliable tool wear monitoring by optimized image and illumination control in machine vision. *Measurement* 28:209–218
6. Lanzetta M (2001) A new flexible high-resolution vision sensor for tool condition monitoring. *J Mater Process Technol* 119:73–82
7. Yang MY, Kwon OD (1996) Crater wear measurement using computer vision and automatic focusing. *J Mater Process Technol* 58:362–367
8. Wang WH, Hong GS, Wong YS (2006) Flank wear measurement by a threshold independent method with sub-pixel accuracy. *Int J Mach Tool Manu* 46(2):199–207
9. Kurada S, Bradley C (1997) A machine vision system for tool wear assessment. *Tribology Int* 30(4):294–304
10. Jurkovic J, Korosec M, Kopac J (2005) New approach in tool wear measuring technique using CCD vision system. *Int J Mach Tools Manu* 45:1023–1030
11. Dawson TG, Kurfess TR (2005) Quantification of tool wear using white light interferometry and three-dimensional computational metrology. *Int J Mach Tool Manu* 45:591–596
12. Mannan MA, Kassim AA, Jing M (2000) Application of image and sound analysis techniques to monitor the condition of cutting tools. *Pattern Recogn Lett* 21:969–979
13. Pavel R, Marinescu J, Deis M, Pillar J (2005) Effect of tool wear on surface finish for a case of continuous and interrupted hard turning. *J Mater Process Technol* 170:341–349
14. Tamizharasan T, Selvaraj T, Noorul Haq A (2006) Analysis of tool wear and surface finish in hard turning. *Int J Adv Manuf Technol* 28:671–679
15. Shahabi HH, Ratnam MM (2007) On-line monitoring of tool wear in turning operation in the presence of tool misalignment. *Int J Adv Manuf Tech*. DOI 10.1007/s00170-007-1119-4
16. Gonzalez RC, Woods RE, Eddins SL (2004) *Digital image processing using Matlab*. Pearson-Prentice Hall, New Jersey
17. Lim JS (1990) *Two-dimensional signal and image processing*. Prentice Hall, Englewood Cliffs, NJ, pp 536–540
18. Otsu N (1979) A threshold selection method from gray-level histograms. *IEEE Trans Syst Man Cybern* 9(1):62–66
19. Gayler JFW, Shotbolt CR (1990) *Metrology for engineers*. Cassell, London
20. Kwon Y, Fischer GW (2003) A novel approach to quantifying tool wear and tool life measurements for optimal tool management. *Int J Mach Tool Manu* 43:359–368

On-line monitoring of tool wear in turning operation in the presence of tool misalignment

H. H. Shahabi · M. M. Ratnam

Received: 3 January 2007 / Accepted: 4 June 2007
© Springer-Verlag London Limited 2007

Abstract A vision system using high-resolution CCD camera and back-light was developed for the on-line measurement of nose wear of cutting tool inserts. Initial study showed that the system is sensitive to several factors in the work environment such as misalignment of cutting tool, presence of micro-dust particles, vibration and intensity variation of ambient light. An algorithm using *Wiener* filtering, median filtering, morphological operations and thresholding was developed to decrease the system error caused by these factors. A conforming method was used to overcome misalignment of the tool insert during offline and on-line measurement. The algorithm, combined with a subtraction method, was applied to measure the nose wear area of the inserts under different machining conditions.

Keywords Machine vision · Tool wear · Wiener filtering · Conforming

1 Introduction

Tool wear during machining operations is known to change the geometry of the cutting tool, thus increasing cutting force, affecting surface finish and decreasing dimensional accuracy of the work piece. Monitoring of tool wear during machining is important to detect problems in the cutting process, assess stability of machining, control surface finish of product and avoid damage to the machine tool itself.

Thus, tool wear has been studied extensively as a significant research area in manufacturing in the past [1–18].

Most of the previous work in tool wear monitoring concerns the measurement of crater wear and flank wear using 2-D and 3-D methods. Crater wear occurs due to the contact of chips with the rake face, while flank wear is due to the rubbing of the work piece with the cutting tool. Measurement of flank and crater wear has been carried out mostly using offline methods due to the nature of the wear area and difficulty in implementing the instruments for on-line measurement. Investigation into the possibility of measuring nose wear for on-line (in-process) tool wear monitoring is limited. Lanzetta [6] measured nose wear offline using a tool fixture and found that the use of profile projection is sufficiently accurate to measure the wear area. A similar technique using back-lighting has been used for extracting the lost material of a cutting tool from its 2-D profile [7].

Tool wear measurement methods can generally be divided into indirect and direct methods. Examples of indirect methods include acoustic emission, tool tip temperature monitoring, vibration signatures (acceleration signals), cutting force monitoring, stress/strain analysis and spindle motor current monitoring. In these methods the optimized signal of the machining process is compared to the live signals. When a live signal deviates from the optimized signal, the system notifies the need to change the cutting tool. The acoustic emission and cutting force measurement methods have been employed to monitor the cutting process in industries [8]. The main advantage of indirect methods is their ability to be applied for on-line tool wear monitoring. Their implementation is, however, not easy due to inadequate knowledge on the effect of tool wear on the signals produced.

Machine vision can be used for directly measuring tool wear because different forms and geometries can be readily

H. H. Shahabi · M. M. Ratnam (✉)
School of Mechanical Engineering, Engineering Campus,
Universiti Sains Malaysia,
14300 Nibong Tebal, Malaysia
e-mail: mmaran@eng.usm.my

identified and measured using suitable algorithms. High accuracy measurement is possible due to the high optical amplification that can be achieved using suitable lenses and the availability of high resolution sensors. Various machine vision methods for measuring tool wear have been proposed in the past, such as automatic focusing for crater wear measurement [9], 2-D edge detection and thresholding to determine flank wear area [10], flank wear observation using textural and gradient operators [11] and tool monitoring using laser scatter [12]. 3-D vision methods have also been used by several researchers to measure tool wear, such as projection of laser raster lines [13], white light interferometry [14, 15] and phase-shifting fringe projection [16]. Others introduced various optical methods for monitoring the tool wear indirectly, e.g., by measuring surface texture and roughness of work piece to predict tool wear [17, 18].

In spite of the advantages of the machine vision system in tool wear measurement and the vast amount of research that has been carried out in the past, their application is limited mainly to laboratories or controlled environment and have not been widely used for on-line monitoring in real production processes. This is partly because the measurement accuracy using high-resolution vision systems is affected by the presence of dust particles, variation in intensity of ambient light and presence of vibration in the workshop area.

On-line tool wear measurement in the past has been limited mainly to CNC machines, where the tool can be parked accurately before an image is captured for the measurement. For instance, Jurkovic et. al. [13] used laser raster line to observe the wear growth pattern on uncoated carbide inserts used on a *Mori Seiki* CNC machine tool. When a vision system is either used for offline wear measurement in the laboratory or on-line measurement on a conventional lathe, accurate positioning of the tool insert is necessary to avoid misalignment errors during image capture. In this work, a vision system for tool wear measurement that is less sensitive to environmental parameters, such as vibration and uncontrolled lighting, and presence of misalignment is proposed. The system was developed offline and later applied for on-line tool wear monitoring.

1.1 Significance of lighting

Lighting is an important factor that affects the quality of captured images in tool wear measurement using machine vision, thus influencing the accuracy of the measurement. The choice of illumination depends on specimen specifications and the output image required. Machine vision lighting used in tool wear measurement can be broadly divided into front-lighting and back-lighting. Back-lighting is used when it is necessary to capture only the contour (silhouette) of the

specimen. This method has been used in the past to extract nose wear from the contour of cutting tool tip [6, 7]. Other researchers [9–12] used front-lighting to study tool wear, though this method is not suitable for measuring nose wear. In this research back-lighting was employed to measure the nose wear area of the cutting tool tip.

2 System configuration

2.1 System setup

A schematic diagram of the system used for tool wear measurement is shown in Fig. 1, and the actual setup for on-line measurement is shown in Fig. 2. A high-resolution CCD camera (Model: *JAI CV-A1*, resolution 1296×1024 pixels) fitted with a 50 mm lens and a 110 mm extension tube was used to capture the image of the tool tip. Back-lighting was used to highlight the profile of the tool. Since the output of the CCD camera is in pixels and the wear area of cutting tool is in mm^2 , it was necessary to determine the horizontal and vertical scaling factors in mm/pixel . The horizontal and vertical scaling factors were obtained using two sphere standard gauges as $1.81 \mu\text{m}/\text{pixel}$ and $2 \mu\text{m}/\text{pixel}$ respectively. The field-of-view of the CCD camera is $2.3 \times 2 \text{ mm}$, and the distance from the front end of camera lens to the cutting tool is approximately 60 mm.

2.2 Machining condition

Various parameters can influence the wear rate of the cutting tool, such as machining time, cutting speed, feed rate, tool material, work piece material and type of coolant. Table 1 shows the parameters used to shape the wear area in this study. The machine used was a conventional lathe machine (Model: *Pinocho S90/200* (Italy)) and the work piece was low-carbon steel bars of 45 mm diameter. The

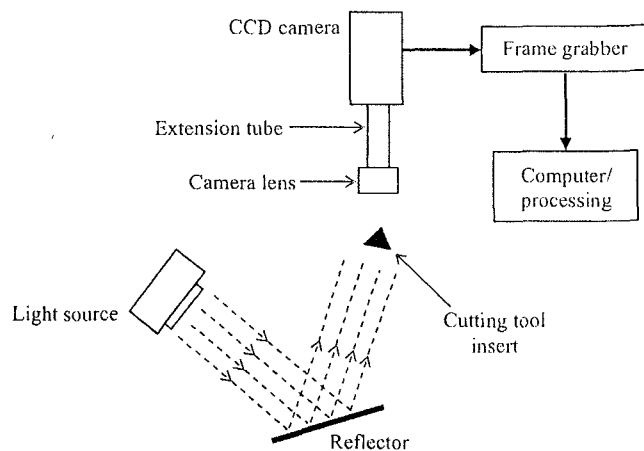


Fig. 1 Schematic diagram of tool wear measurement system

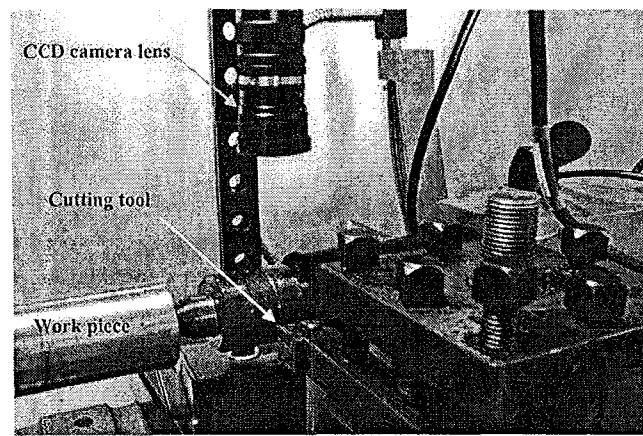


Fig. 2 Actual setup of on-line tool wear measurement system

cutting tools were uncoated carbide inserts manufactured by Sandvik Co. Ltd. (Sweden). Three cutting speeds and four machining durations, i.e., 10 min, 20 min, 30 min and 40 min, were used to monitor the growth of wear area of the cutting tool insert.

3 Wear measurement algorithm

The various stages involved in the measurement of nose wear area are shown in Fig. 3, and are described below.

3.1 Image acquisition

In Stage 1, a frame-grabber (*data translation-DT3162*) was used to interface the CCD camera to the computer. Output of the camera was captured using the frame grabber. In this study, it is important to ensure sharpness of image captured because blurring decreases the accuracy of measurement. The sharpness of image was ensured using the intensity profiles

across the image, whereby a sharp image produced maximum intensity gradient between the bright and dark regions.

3.2 Image enhancement

In Stage 2, the images were enhanced using noise filtering methods. The captured image $g(x, y)$ can be represented by:

$$g(x, y) = f(x, y) + \eta(x, y) \quad (1)$$

where $f(x, y)$ is the original image, and $\eta(x, y)$ is the noise term in the image.

Median filtering and *Wiener* filtering were used to recover the images of cutting tools that were degraded by noise. Median filtering is a method used to remove impulse noise without blurring the image. This method replaces the current pixel by the median of neighborhood pixels within a mask. Compared to other filtering methods, median filtering maintains the edge details in the original image while reducing noise [19]. The *Wiener* filtering method is an early method used to recover images corrupted by noise [20]. This method is one of the best approaches to recover the images and it is not sensitive to inverse filter of noise.

Figure 4 (a)–(c) show the effect of applying median filtering on the intensity profile across the tool insert. Figure 4 (b) shows the intensity profile after median filtering using a 3×3 window and Fig. 4 (c) shows the optimum intensity profile obtained using a 10×10 window. Since different filter mask sizes produced different results, a total of 10 masks ranging from 2×2 to 11×11 were used to determine the optimum mask size. Figure 4 (d) shows the effect of using *Wiener* filtering on the intensity profile. Figure 5 shows the wear area of the cutting tool insert before filtering (Fig. 5 (a)), after applying median filtering (Fig. 5 (b)) and after applying *Wiener* filtering (Fig. 5 (c)). Although the results after applying median and *Wiener* filtering look almost alike, there is a finite difference in the wear areas.

3.3 Morphological operation

In Stage 3 of the algorithm, morphological operations were used to smooth the images by removing pixels due to micro-dust particles. The opening and closing operations are the most basic morphological operations, obtained by combining the dilation and erosion operations [21]. These operations were used to smooth the contour of a cutting tool shown in Fig. 6 (a). Figure 6 (b) is the magnified area A of Fig. 6 (a). The boundary line of the cutting tool is not a straight line due to the presence of micro-dust particles. The dust particles manifest as small 'protrusions' and 'notches' in the tool tip. Figure 6 (c) shows that the notches in area A were removed after applying opening operation, and Fig. 6 (d) shows that protrusions were removed as well after applying

Table 1 Machining parameters

Machine tool	Conventional lathe (<i>Pinocho S90/200</i>)
Work piece	Non-alloy steel rod St37
Cutting tool	Uncoated cemented carbide: <i>TPUN-16-04-04-H13A</i> Sandvik Co. Ltd., Sweden
Feed rate	0.25 mm/rev
Machining depth	0.5 mm
Cutting speed	134, 163, 191 m/min
Coolant	Air
Machining duration	10 min 20 min 30 min 40 min

Fig. 3 Flow chart of algorithm used for tool wear measurement

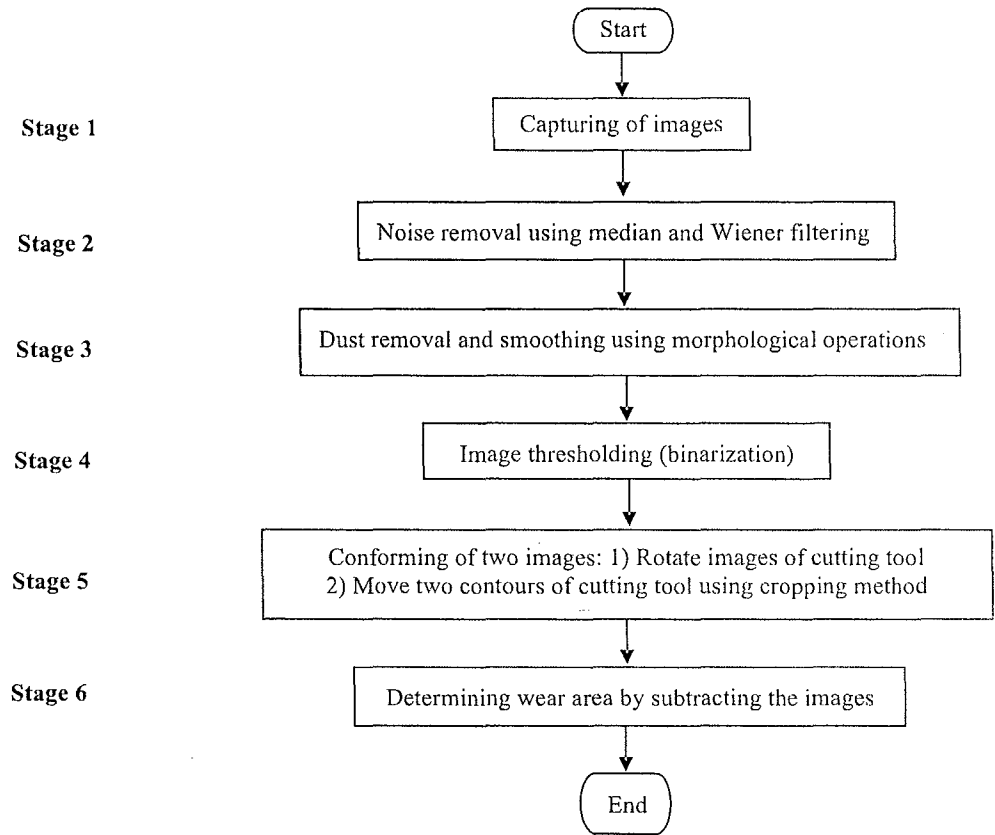


Fig. 4 Intensity profile across tool: (a) Before filtering (original), (b) after median filtering (non-optimum), (c) median filtering (optimum) and (d) *Wiener* filtering (optimum)

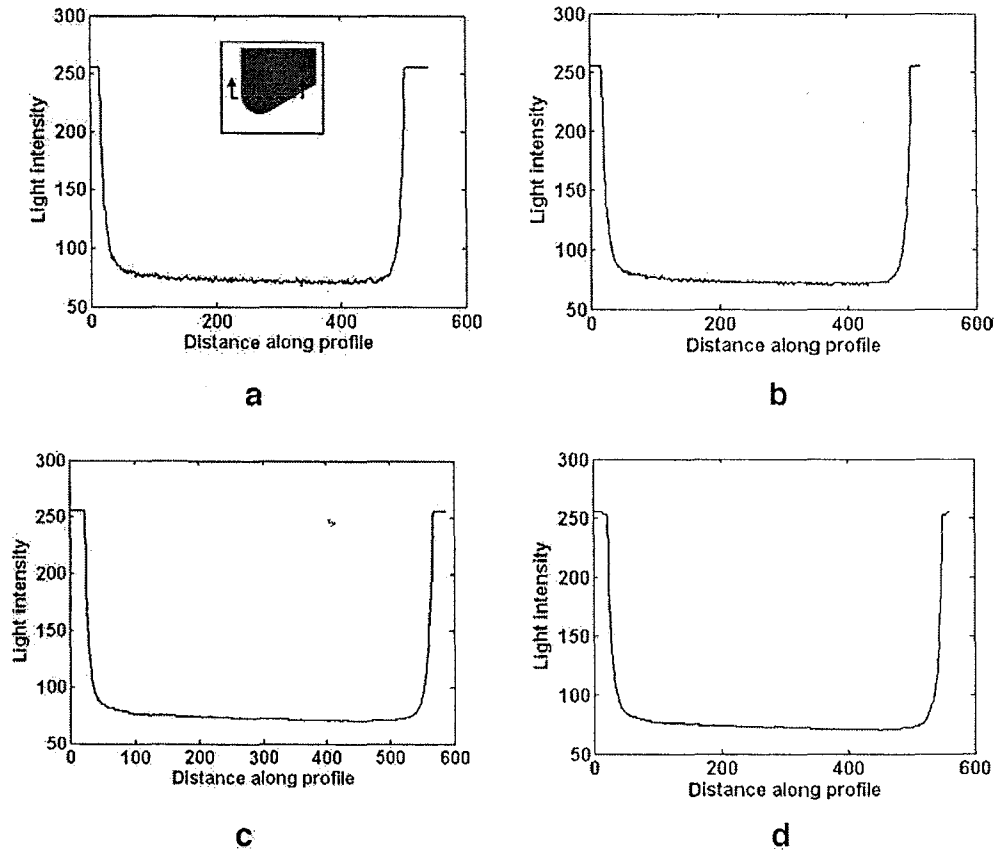
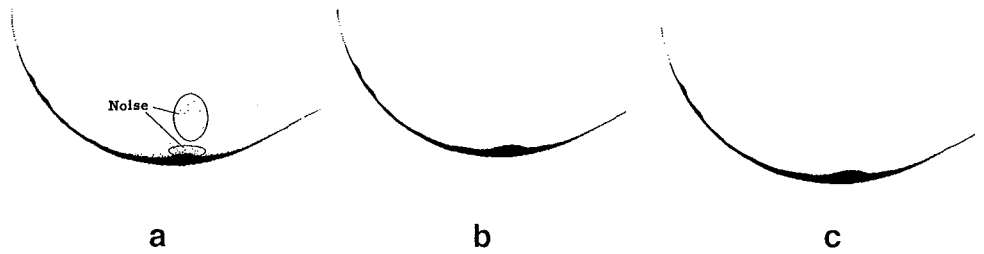


Fig. 5 Subtracted images: (a) Before removing noise, (b) after removing noise by median filtering and (c) after removing noise by *Wiener* filtering



the closing operation. For both operations a 3×3 structuring element was found to be sufficient to remove the dust particles.

3.4 Segmentation

In stage 4, the image was segmented to separate the tool tip from the background using the thresholding method. Thresholding produces a binary image by setting all pixels in the input image for a given range of gray values to 1 and the remaining values to 0. A thresholding parameter (T) is used to define the range of gray scale pixels that are set to value 0 and 1. The simple thresholding method can be defined by

$$g(x,y) = \{1 \text{ if } f(x,y) \geq T\} \text{ or } \{0 \text{ if } f(x,y) < T\} \quad (2)$$

where $f(x,y)$ is the input image. T was determined from the image gray level histogram.

3.5 Conforming

In stage 5, a conforming method was used to correct misalignment of the tool insert. In the offline measurement, a tool holder was used to fix the cutting tool in the fixture shown in Fig. 2. After capturing the image of unworn cutting tool, it was necessary to remove the cutting tool from the tool holder to use it on the lathe machine. After machining, the worn cutting tool was refastened onto the holder to capture an image of the worn tool. Due to a small clearance

in the tool holder, rotational and translational misalignment between the unworn and worn tool occur when the tool is removed and refastened. In the on-line measurement, movement of cutting tool during machining causes similar misalignment due to machine parts clearance. For accurate tool wear measurement it is necessary to correct the misalignment. To achieve this, an unworn cutting tool was fastened in the tool holder and an image was captured. The tool was removed, refastened and a second image was captured. The effect of cutting tool movement caused by the clearance in the tool holder is shown in Fig. 7 obtained by subtracting two successive images.

To investigate the effect of tool holder clearance on positioning error, 21 images were captured from one cutting tool, each time the tool was removed and refastened in its holder. Each image was subtracted from the first image and the results of 20 subtractions were recorded as test results. The rest of this section describes the algorithm used to decrease the misalignment error using the conforming method. In this work, 'conforming' means rotating and translating two images of cutting tool contour to nullify misalignment of the tool when the images are captured.

The orientation of the cutting tool tip can be detected automatically by software method in order to move and conform the first captured image of cutting tool to the second. Figure 8 shows two binary images of tool tip where the misalignment is clearly visible. α_1 and α_2 are the angles of the upper left side of the tool tip from the vertical as shown in the figure. One of the conditions for the two images to conform together is $\alpha_1 = \alpha_2$. The other condition is that the

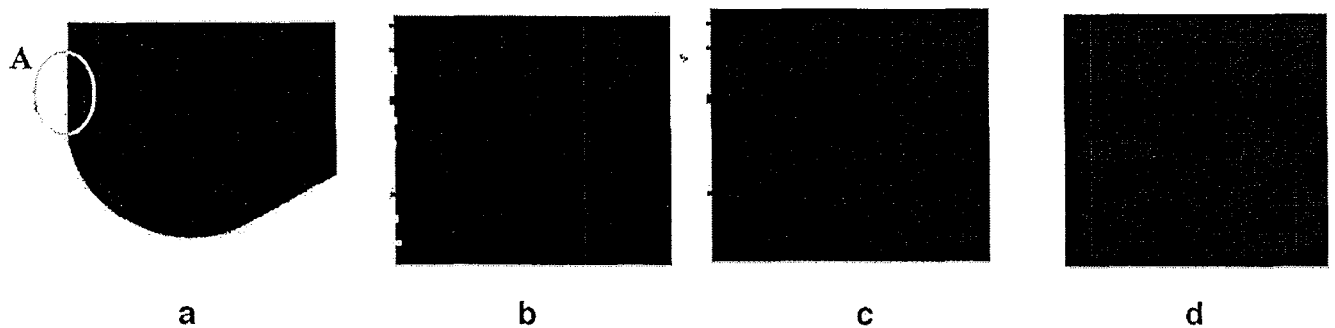


Fig. 6 Removal of micro-dust using opening and closing operations: (a) Cutting tool tip, (b) area A before opening, (c) area A after opening, (d) area A after opening and closing

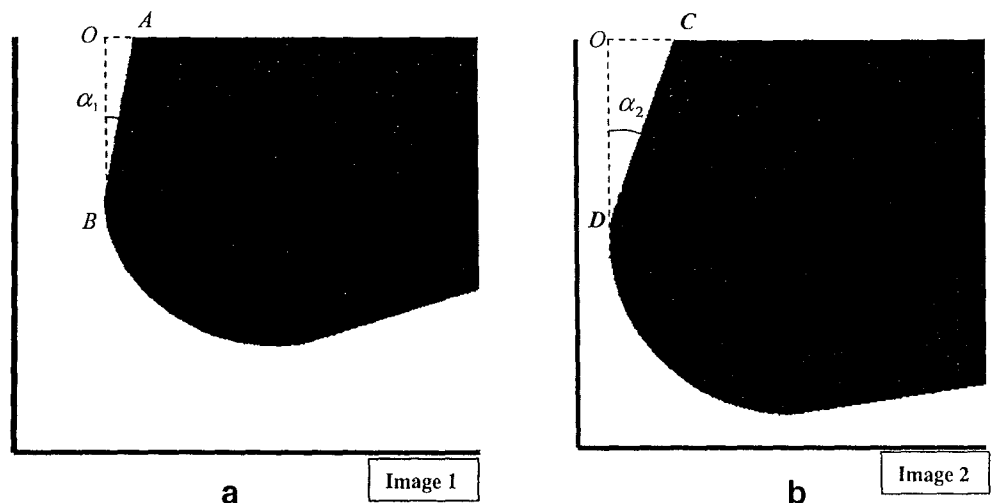


Fig. 7 Result of subtraction of two images before applying the conforming method

distances from the edges of the image to the tool tip in the first image (Image 1) must be equal to those for the second (Image 2). The conforming method comprises the following stages as applied to Image 1 and Image 2 shown in Fig. 8:

- Stage 1 Detect pixels on line *A–B* in Image 1 and line *C–D* in Image 2.
- Stage 2 Determine the best-fit line for pixels on *A–B* and *C–D* using least-squares approximation. The fitted lines are denoted as *A–B* and *C–D*.
- Stage 3 Determine angles α_1 and α_2 between lines *A–B*, *C–D* and the vertical.
- Stage 4 Rotate Image 1 and Image 2 using *Imrotate* in *Matlab* through α_1 and α_2 respectively.
- Stage 5 Crop both images to trim the black pixels added at the edges due to rotation (Fig. 9).
- Stage 6 Detect distances D_{1X} , D_{2X} and D_{1Y} , D_{2Y} between image contours and axes (Fig. 9).
- Stage 7 Crop two images to conform one with the other (equivalent to translating one image to conform to another).

Fig. 8 Binary images (Image 1 and Image 2) before using conforming method



In Stage 1 of the conforming algorithm, all pixels that lie on the lines *A–B* and *C–D* in Fig. 8 were detected. In theory, these pixels should lie on a straight line, but in reality they do not. This is due to the quantization error in the digitized image. In stage 2, the least-squares method was used to determine the best fitted line between these pixels. The coordinates of the end points of the best fit lines are $A'(X1, Y1)$ and $B'(X2, Y2)$ in Image 1 and $C'(X3, Y3)$ and $D'(X4, Y4)$ in Image 2.

In stage 3, angles α_1 and α_2 were determined as follows:

$$\alpha_1 = \tan^{-1} \left(\frac{OA'}{OB'} \right) \tag{3}$$

$$\alpha_2 = \tan^{-1} \left(\frac{OC'}{OD'} \right) \tag{4}$$

where

$$OA' = \Delta X_1 = X_1 - X_2 \tag{5}$$

$$OB' = \Delta Y_1 = Y_1 - Y_2$$

(5)and

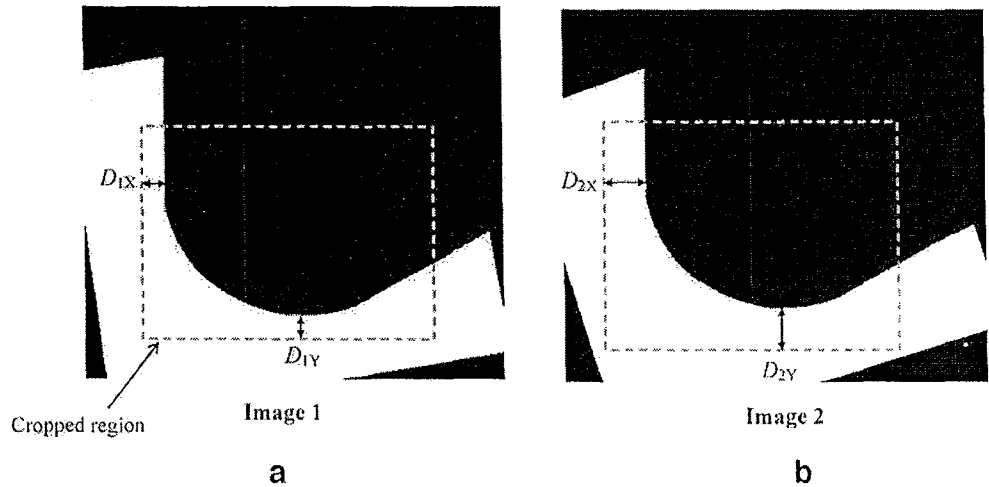
$$OC' = \Delta X_2 = X_3 - X_4 \tag{6}$$

$$OD' = \Delta Y_2 = Y_3 - Y_4$$

In stage 4, the first and second images were rotated using *Imrotate* command in *Matlab* by α_1 and α_2 , respectively. The default rotation direction is counterclockwise. If ΔX_1 and ΔX_2 are positive, the images are rotated counterclockwise, otherwise they are rotated clockwise. Figure 9 shows the two images after rotation. Due to the slightly different rotation angles, the areas of the black pixels added by the rotation are clearly different in the two images shown.

In stage 5, the two images were cropped to trim the black pixels at the sides added to the images by rotation. In

Fig. 9 Image 1 and Image 2 after rotation (region to be cropped is shown in dotted line)



stage 6, distances D_{1X} , D_{2X} and D_{1Y} , D_{2Y} in the rotated and cropped images were determined. In stage 7, one of the images is cropped further by distances given by:

$$\Delta D_X = |D_{1X} - D_{2X}| \quad (7)$$

and

$$\Delta D_Y = |D_{1Y} - D_{2Y}| \quad (8)$$

If $D_{2X} > D_{1X}$ Image 2 is cropped, whereas if $D_{2X} < D_{1X}$ Image 1 is cropped. The size of the crop window is maintained by adding a distance equal to ΔD_X on the opposite side of the image. The same method was used for the other two sides of the window.

Figure 10 shows the final images after applying the conforming method. To determine the system error, the absolute difference between Image 1 and Image 2 after conforming was determined and shown in Fig. 11. Comparison of Fig. 11 with Fig. 7 clearly shows that the error due to tool misalignment is greatly reduced after applying the conforming method.

4 Verification of wear area using optical microscope

The captured images show the cutting tool contours and from these images the area of cutting tool tips can be determined. The cutting tool tips are worn during the machining process, and nose wear decreases the area of cutting tool tips. By subtracting



Fig. 10 Image 1 and Image 2 after conforming

the worn cutting tool image from the original image, the wear area can be determined. Figure 12 (a)–(c) show the wear area after subtracting the worn cutting tool tips for 40 min machining duration from the original image. The subtraction was carried out after applying the conforming method discussed in the foregoing section.

The wear area of cutting tool determined using the proposed method was verified using an optical microscope (*Ken-A-Vision* (USA)) with a magnification of 100. A CCD camera (*Ken-A-Vision 7100*, resolution 320×240 pixels) fitted with an 8 mm lens and mounted onto the microscope was used to capture the image of the tool tip. Back-lighting available in the system was used to highlight the contour of the specimen. A 0.25 mm pin gauge (*Mitotoyo*) was initially focused under the microscope and the diameter was measured in pixels using the CCD camera. The horizontal and vertical scaling factors were found to be

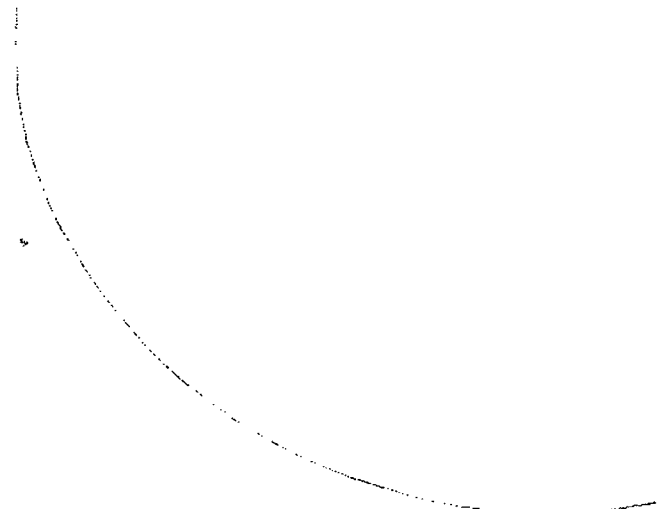
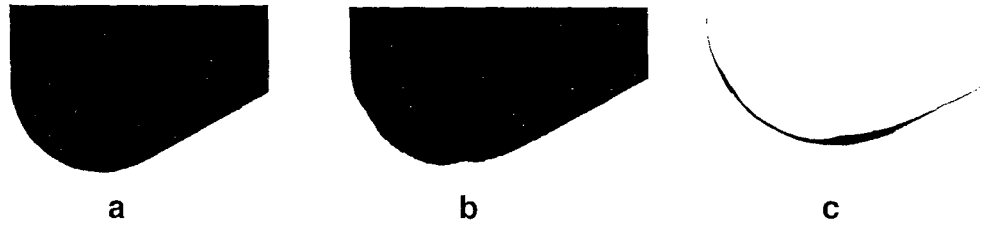


Fig. 11 Result of subtraction of Image 1 and Image 2 after applying conforming method

Fig. 12 (a) Unworn cutting tool tip, (b) worn cutting tool tip after 40 minutes of machining, (c) wear area obtained by subtraction



3.3 $\mu\text{m}/\text{pixel}$ and 2.8 $\mu\text{m}/\text{pixel}$, respectively. The field-of-view of the CCD camera is 1.06 mm \times 0.672 mm.

Four different cutting tool tips were used to verify the results of the on-line measurement. A grinding machine was used to deliberately introduce 'wear' on the cutting tool tips for the verification purpose. Images of four different cutting tool tips were captured before and after grinding using the on-line vision method and the optical microscope. Comparison of the wear areas of cutting tool tips determined using the algorithm developed in this study and those measured using the microscope showed a maximum deviation of 6.8%.

5 Results of wear measurement

The results of wear measurement are presented in three parts. In sub-section 5.1, the system error before and after applying the conforming algorithm developed in this study is presented. In sub-section 5.2, results of the study on the effect of ambient light intensity and ambient vibration on system error is discussed, and in sub-section 5.3 the results of on-line measurement of the wear area of cutting tool using the system developed in this work is presented.

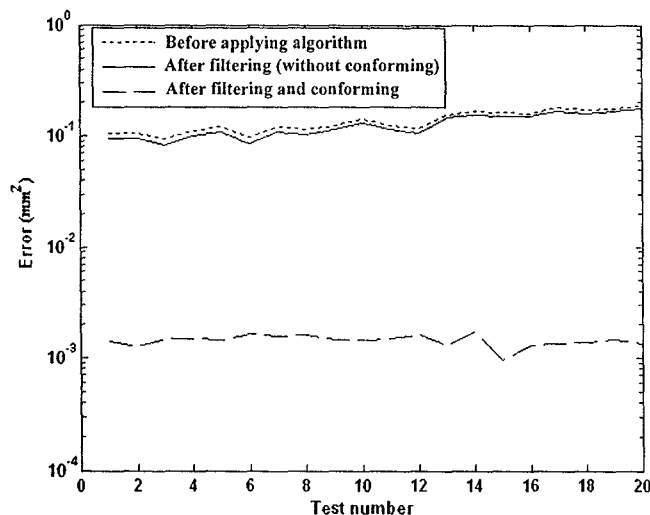


Fig. 13 The system error before and after applying the conforming algorithm

5.1 System error evaluation

The algorithm developed was used to determine the effect of tool holder and machine parts clearance on the misalignment error of the cutting tool. The images captured using backlighting comprises two regions—the background and the tool tip. Since the images are in grayscales, the intensity of the background and tool tip varied between 0 and 255. Intensity histograms of the images were used to find the threshold T for thresholding (binarizing) the image. Thresholding changes the intensity of background to 1 and that of the cutting tool to 0 and, therefore, effectively removes the effect of ambient lighting that causes non-uniform intensity distribution in the image. The two images of one cutting tool insert were subtracted before and after applying the conforming method as described earlier.

Figure 13 shows the results of subtracting 20 different images of one cutting tool before and after applying the conforming method. In each case, the tool was removed and refastened onto the tool holder. Each of the images was subtracted from the first image (reference). The maximum and minimum errors (in pixels) were, respectively, 25,924 and 51,696 before applying the algorithm consisting of filtering, morphological and conforming operations. By applying the scaling factors, these errors correspond to

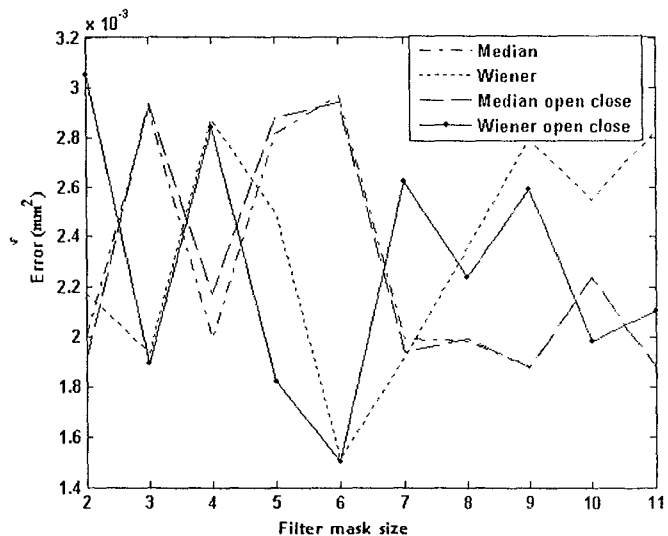


Fig. 14 System error of subtracting two images of one cutting tool using different filter mask size

Table 2 Wear area of cutting tools ($\times 10^{-6}$ mm²)

Cutting speed (m/min)	Machining duration (min)			
	10	20	30	40
191	3149	5032	6136	9785
163	6161	6585	10820	13611
134	7616	9213	19436	26879

93.85×10^{-3} mm² and 187.14×10^{-3} mm² respectively. The minimum and maximum errors after applying the algorithm are 0.95×10^{-3} mm² and 1.71×10^{-3} mm², respectively. The maximum reduction in error using the proposed algorithm is 99.4%. Figure 13 also shows that there is a slight reduction in the pixel area in the subtracted image as a result of the filtering and morphological operations. This is due to the removal of noise and dust particles in the image. The number of pixels remaining after applying the proposed algorithm is suspected to be due to other system errors, such as vibration and limitation of camera resolution. The mean error due to the remaining pixels is 1.45×10^{-3} mm².

In this work, Median and *Wiener* filtering were employed to remove noise, and morphological operations were used to remove the micro-dusts particles. The larger dust particles can be removed using compressed air, but removal of micro-dusts in the workshop area is difficult. The subtraction results were found to be influenced by different mask sizes used in the filtering operations. Therefore, it was necessary to use an iterative approach to get the optimum result using median and *Wiener* filtering. The optimum result is considered achieved when the subtracted area is a minimum. A program written in *Matlab* was used to change the mask size automatically to find the optimum result. Figure 14 shows the results of subtracting two images of one cutting tool using different square mask sizes after applying the conforming algorithm to correct misalignment. The results show that the system error varies randomly using either median or *Wiener* filter, both with and without the morphological operations. The minimum error occurs with *Wiener* filtering using a 6×6 mask. In all cases, a 3×3 structuring element was used for the morphological operations. The study was repeated for 20 different images of one cutting tool insert. The data plotted in Fig. 13 was obtained using the filter mask that gave the optimum result.

5.2 Effect of ambient lighting and ambient vibration

5.2.1 Effect of ambient lighting

To study the effect of ambient lighting on the system error, two different images of one cutting tool tip were captured

under different ambient light intensity. A light meter (*Lx-101A*, *LT Lutron*) was used to record the ambient light intensity. The light intensity of the ambient was 16 lux and 1321 lux when capturing the first image and second image, respectively. The images were subtracted to determine the system error in the presence of different ambient light intensities. The system error due to different ambient light intensity was found to be 1.48×10^{-3} mm². Since this error falls within the range of minimum and maximum error under the same lighting condition, the system can be considered relatively insensitive to environmental light intensity, provided the intensity is not too high.

5.3 Effect of ambient vibration

To study the effect of ambient vibration on the system error, 21 different images of one cutting tool tip were captured under the same ambient light. Each of the 20 images was subtracted from the first image one at a time. The system error due to ambient vibration was found 2×10^{-3} mm². Since this error also falls within the range of minimum and maximum error under the same lighting condition, the system can be considered relatively insensitive to environmental vibration.

5.4 Measurement of nose wear area

To determine the nose wear area of cutting tools, uncoated carbide inserts were used to machine low-carbon steel rods using a conventional lathe machine. Images of the cutting tool inserts were captured on-line before machining. The inserts were then used to machine the work piece. The cutting speeds were changed for each machining duration as shown in Table 1. Images of the worn inserts were then captured on-line for different machining durations. Each of the images

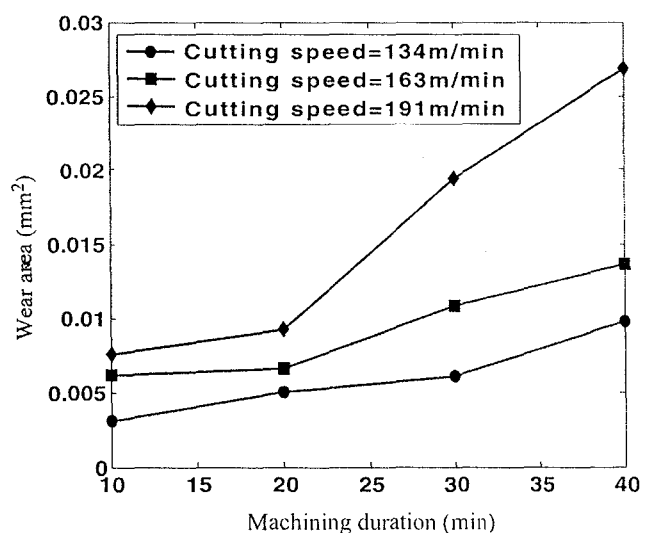


Fig. 15 Wear area of cutting tools for various machining time and cutting speed

was subtracted from its unworn image by applying the algorithm developed in this work. Table 2 shows the results of wear area measurement for three different cutting tool inserts. Figure 15 shows a plot of the wear area for three different cutting speeds for different machining duration. The results show that the nose wear area increases with machining duration as expected. For a given machining duration, the wear also increases with cutting speed. This result is in agreement with those published previously using offline measurement method [7].

Unlike past research where tool wear measurement was carried out offline or on-line using a CNC lathe, where accurate parking of cutting tool is possible, in this study the wear area was measured on-line on a conventional lathe machine. Misalignment of cutting tool was overcome using the proposed conforming algorithm. The filtering and morphological operations in the proposed algorithm also remove image noise and micro-dust particles, thus making the technique sufficiently robust for workshop applications.

6 Conclusion

A method of on-line monitoring of nose wear of cutting tool insert that is less sensitive to environmental parameters such as misalignment of cutting tool, presence of micro-dust and various intensities of ambient light and vibration has been developed in this research. An algorithm that employs filtering and morphological operations together with a conforming method effectively reduces errors caused by the environmental factors. Median and *Wiener* filtering were used to remove noise in the image, and the morphological closing and opening operations were used to reduce errors caused by micro-dust particles present on the cutting tool insert.

The proposed machine vision system using back-lighting is able to measure the nose wear area of cutting tool insert from the tool contour. Results of study on unworn cutting tool insert showed that the system error caused mainly by misalignment of the cutting tool insert decreased up to 99.4% after applying the algorithm. The proposed technique and algorithm developed in this study increases the ability of machine vision system for application outside of the laboratory where misalignment of cutting tool, dust particles, unpredictable lighting, and vibration may exist.

Acknowledgement The authors would like to thank Universiti Sains Malaysia for the offer of the USM short-term grant that enabled this work to be carried out.

References

- Sortino M (2003) Application of statistical filtering for optical detection of tool wear. *Int J Mach Tools Manuf* 43:493–497
- Pfeifer T, Wieggers L (2000) Reliable tool wear monitoring by optimized image and illumination control in machine vision. *Measurement* 28:209–218
- Jun Z, Jianxin D, Jianhua Z, Xing A (1997) Failure mechanisms of a whisker-reinforced ceramic tool when machining nickel-based alloys. *Wear* 208(1–2):220–225
- Ezugwu EO, Bonney J (2004) Effect of high-pressure coolant supply when machining nickel-base, Inconel 718, alloy with coated carbide tools. *J Mater Process Technol* 153–154:1045–1050
- Kassim AA, Mian Z, Mannan MA (2004) Connectivity oriented fast Hough transform for tool wear monitoring. *Pattern Recognit* 37:1925–1933
- Lanzetta M (2001) A new flexible high-resolution vision sensor for tool condition monitoring. *J Mater Process Technol* 119:73–82
- Kwon Y, Fischer GW (2003) A novel approach to quantifying tool wear and tool life measurements for optimal tool management. *Int J Mach Tools Manuf* 43:359–368
- Dimla DES (2000) Sensor signals for tool wear monitoring in metal cutting operations-A review of methods. *Int J Mach Tools Manuf* 40:1073–1098
- Yang MY, Kwon OD (1996) Crater wear measurement using computer vision and automatic focusing. *J Mater Process Technol* 58:362–367
- Wang WH, Hong GS, Wong YS (2006) Flank wear measurement by a threshold independent method with sub-pixel accuracy. *Int J Mach Tools Manuf* 46(2):199–207
- Kurada S, Bradley C (1997) A machine vision system for tool wear assessment. *Tribol Int* 30(4):294–304
- Wong YS, Nee AYC, Li XQ, Riesdorf C (1997) Tool condition monitoring using laser scatter pattern. *J Mater Process Technol* 63:205–210
- Jurkovic J, Korosec M, Kopac J (2005) New approach in tool wear measuring technique using CCD vision system. *Int J Mach Tools Manuf* 45:1023–1030
- Dawson TG, Kurfess TR (2005) Quantification of tool wear using white light interferometry and three-dimensional computational metrology. *Int J Mach Tools Manuf* 45:591–596
- Devillez A, Lesko S, Mozer W (2004) Cutting tool crater wear measurement with white light interferometry. *Wear* 256:56–65
- Wang WH, Wong YS, Hong GS (2006) 3D measurement of crater wear by phase shifting method. *Wear* 261(2):164–171
- Mannan MA, Kassim AA, Jing M (2000) Application of image and sound analysis techniques to monitor the condition of cutting tools. *Pattern Recognit Lett* 21:969–979
- Choudhury SK, Bartarya G (2003) Role of temperature and surface finish in predicting tool wear using neural network and design of experiments. *Int J Mach Tools Manuf* 43:747–753
- Galbiati LJ (1990) *Machine vision and digital image processing fundamentals*. Prentice-Hall, Upper Saddle River, NJ, USA
- Gonzalez RC, Woods RE, Eddins SL (2004) *Digital image processing using Matlab*. Pearson-Prentice Hall, Upper Saddle River, NJ, USA
- Gonzalez RC, Woods RE (2002) *Digital image processing*. Pearson Education, Upper Saddle River, NJ, USA

Notch wear detection in cutting tools using gradient approach and polynomial fitting

H. H. Shahabi · T. H. Low · M. M. Ratnam

Received: 5 June 2007 / Accepted: 8 February 2008
© Springer-Verlag London Limited 2008

Abstract Cutting tool wear is well known to affect the surface finish of a turned part. Various machine vision methods have been developed in the past to measure and quantify tool wear. The two most widely measured parameters in tool wear monitoring are flank wear and crater wear. Works carried out by several researchers recently have shown that notch wear has a more severe effect on the surface roughness compared to flank or crater wear. In this work, a novel gradient detection approach has been developed to detect the presence of micro-scale notches in the nose area of the cutting tool. This method is capable of detecting the location of the notch accurately from a single worn cutting tool image.

Keywords Notch wear · Cutting tool · Gradient detection · Polynomial fitting

1 Introduction

Vision-based systems are gaining considerable attention from the research community for tool wear measurement due to their numerous advantages, such as direct measurement of wear, non-contacting, high spatial resolution, high-speed data processing, visualization of wear area, etc. Kurada et al. [1] gave a review of the basic principles, instrumentation and processing schemes used in various machine vision sensors. Two of the most common types of tool wear measured are flank wear and crater wear [2].

Flank wear occurs on the relief face of the cutting tool and is mainly caused by the rubbing action of the tool on the machined surface, while crater wear occurs on the rake face of the tool. The criteria for tool life is based on the width of the flank wear land defined in the ISO3685 standard [3]. According to the standard, the maximum width of the flank wear land $VB_{Bmax}=0.6$ mm if the flank wear is not regularly worn. If the flank wear land is regularly worn, the criteria for tool life is the average width of the flank wear land $VB_B=0.3$ mm.

Several researchers used machine vision methods to measure the flank wear directly in the past. For instance, Kurada et al. [2] used a series of image processing operations that include image enhancement by linear and median filtering, segmentation using edge operators and feature extraction to measure the maximum wear land width. Wang et al. [4] measured flank wear using a threshold-independent edge-detection approach based on moment invariance. In another publication, Wang et al. [5] measured flank wear by capturing and processing successive images of a moving cutting tool. Pfeifer et al. [6] extracted the flank wear contour using optimized adjustment of illumination, while Sortino [7] used a statistical filtering method to detect the worn edge of the cutting tool. Jeon et al. [8] used real-time vision technology to monitor the average and maximum peak values of the wear land.

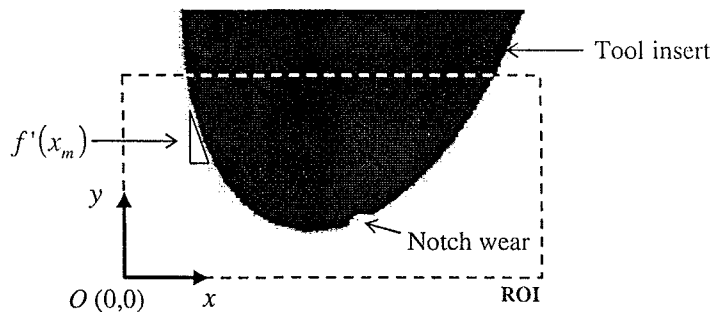
Unlike flank wear, measurement of crater wear has received less attention in the past. Wang et al. [9] applied the phase-shifting method using fringe projection to extract the 3-D wear crater profile, while Jurkovic et al. [10] measured both crater wear and flank wear using structured lighting.

Although flank wear has been extensively studied in the past, Ghani et al. [11] have shown experimentally that for some machining conditions the surface roughness of the

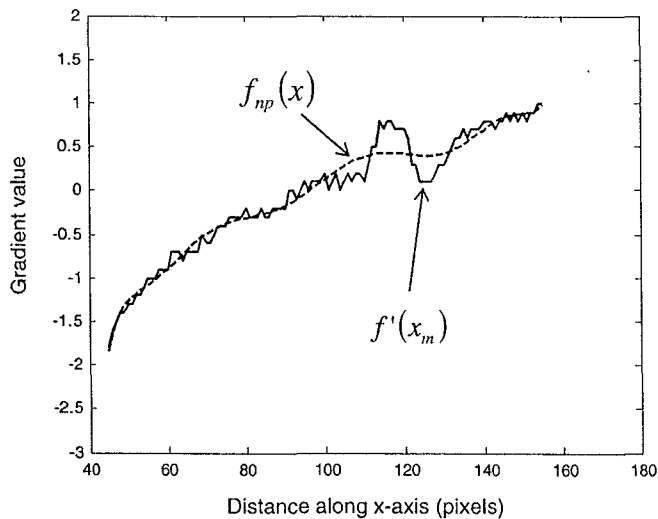
H. H. Shahabi · T. H. Low · M. M. Ratnam (✉)
School of Mechanical Engineering, Engineering Campus,
University Sains Malaysia,
14300 Nibong Tebal, Malaysia
e-mail: mmaran@eng.usm.my

workpiece remained almost constant in spite of the increase in flank wear with increase in cutting speed, feed rate and depth of cut. At a certain feed rate the surface roughness even decreased with the increase in flank wear. Pavel et al. [12] also reported that the surface roughness decreased with time in interrupted cutting. However, for continuous cutting, the surface roughness increased. The increase in roughness was attributed to increase in notch wear that develops into a steep groove at the cutting edge. Since cutting tools can develop different wear patterns under different cutting condition but have the same VB_{Bmax} value, the use of VB_{Bmax} as a criterion to define tool wear is questionable. Kwon et al. [13] proposed a new tool wear index that takes into account both flank wear and nose wear areas. The nose wear was measured using 2-D projection of the nose profile. Although the surface roughness was found to increase with material loss due to tool wear, it is difficult to make a direct comparison between the two because the material loss may originate from a region of the tool not directly in contact with the finished surface.

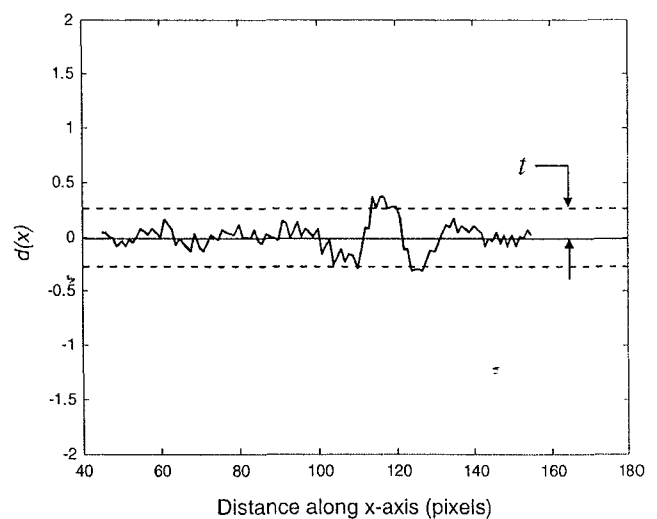
When workpiece surface finish quality is the main interest in machining, the correct tool wear parameter must be used to study the effect of wear on the surface roughness. Since the tool tip is directly in contact with the workpiece during machining, the workpiece surface profile will depend directly on the geometry of the tool tip. As the tool wears, the contact geometry changes, thus affecting the surface being machined. If notches appear in the cutting tool tip, the surface quality will be seriously affected. Thus, early detection of the presence of notch wear is extremely important to ensure high product surface quality. Previous study on the effect of notch wear on surface roughness was carried out by removing the cutting tool and observing it in the laboratory using a stereo microscope [12]. This procedure, however, is not practical in real machining applications. The objective of this study is to develop a non-contact vision based method that can be used to detect notch wear from a single image of cutting tool in the micrometer range. The system developed can be implemented in the machine for in-cycle monitoring of the



a



b



c

Fig. 1 (a) Simulated image to cutting tool having notch defect, (b) plot of gradient values along profile and polynomial fitting, (c) plot of difference $d(x)$ against distance along x -axis

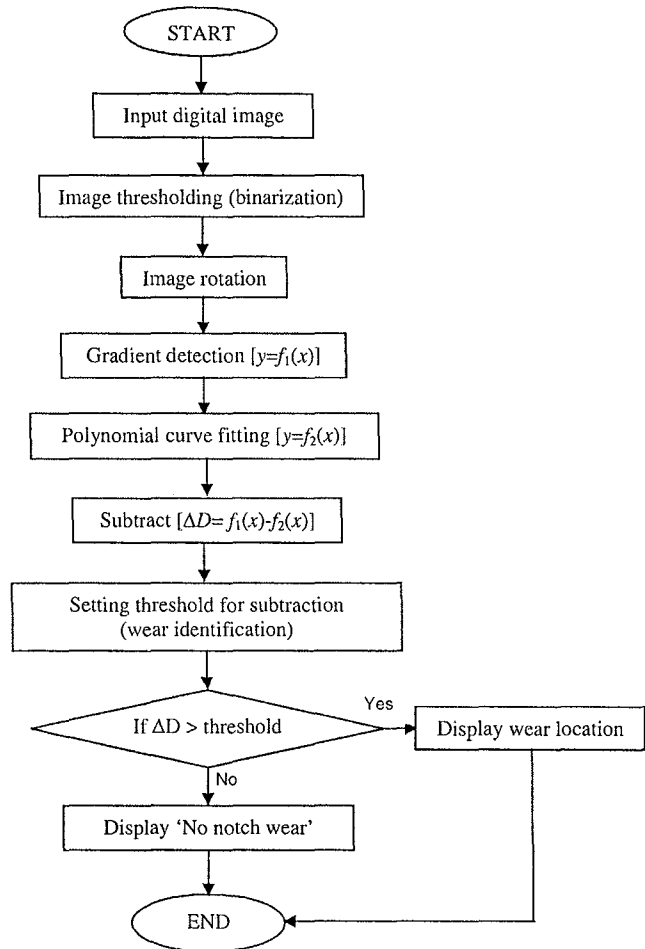


Fig. 2 Flow chart of algorithm used to determine notch location

cutting tool, i.e., without removing the tool from the machine.

2 Theory of notch wear detection using gradient approach

Figure 1 (a) shows the 2-D profile of the tip of a simulated image of a 'cutting tool' having notch wear. If the profile

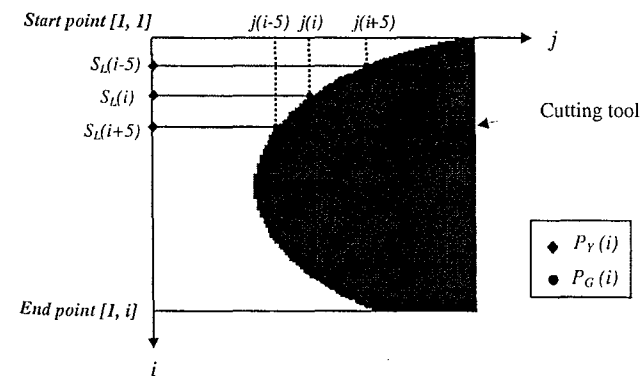


Fig. 3 Scanning method to determine gradient at tool edge

within the region of interest (ROI) can be estimated using the continuous polynomial function of order-*n*,

$$f(x) = a_0 + a_1x + a_2x^2 + \dots + a_nx^n \tag{1}$$

the gradient $f'(x)$ at each point on the profile will be given by

$$f'(x) = a_1 + 2a_2x + \dots + na_nx^{n-1} \tag{2}$$

Since the data for a digitized image exist only in a discrete form, the gradient can be approximated by the following equation:

$$f'(x_m) = \frac{f(x_m + p) - f(x_m - p)}{2p} \tag{3}$$

where *p* is the step length in pixels.

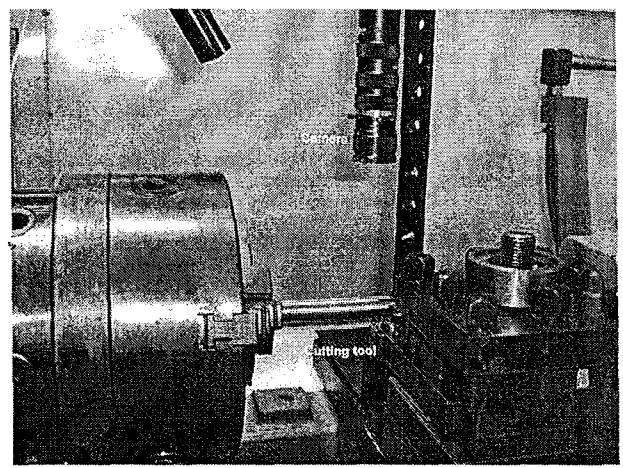
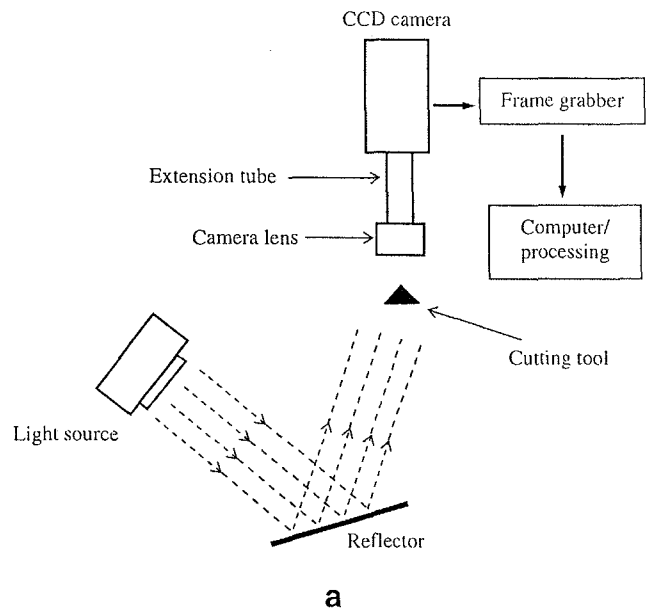


Fig. 4 (a) Schematic diagram of the vision system setup, (b) photograph of the setup on the lathe machine

Table 1 Machining parameters

Machine tool	Conventional lathe machine: Model: <i>Pinocho S90/206</i>	
Work piece	Steel rod AISI 1035 (0.32–0.38% C, 98.63–99.09% Fe, 0.6–0.9% Mn, 0.04% P (max), 0.05% S(max))	
Cutting tool	Uncoated cemented carbide: TPUN-16-03-04_H13A, Sandvik Co, Ltd, Sweden	
Feed rate	0.25 mm/rev	0.25 mm/rev
Machining depth	0.5 mm	0.5 mm
Cutting speed	134 m/min	190 m/min
Coolant	Air	Air
Machining time	0–40 min	0–40 min

Figure 1 (b) shows the gradient $f'(x_m)$ extracted from the simulated image of a worn cutting tool using $p=5$. The presence of a notch defect causes a change in the gradient profile and can be easily visualized from the figure. The small fluctuations of the gradient values along the profile

are due to the discretization of the image. If the 'defect' gradient profile is fitted with a n -th order polynomial function $f_{np}(x)$, then the difference

$$d(x) = f'(x_m) - f_{np}(x) \quad (4)$$

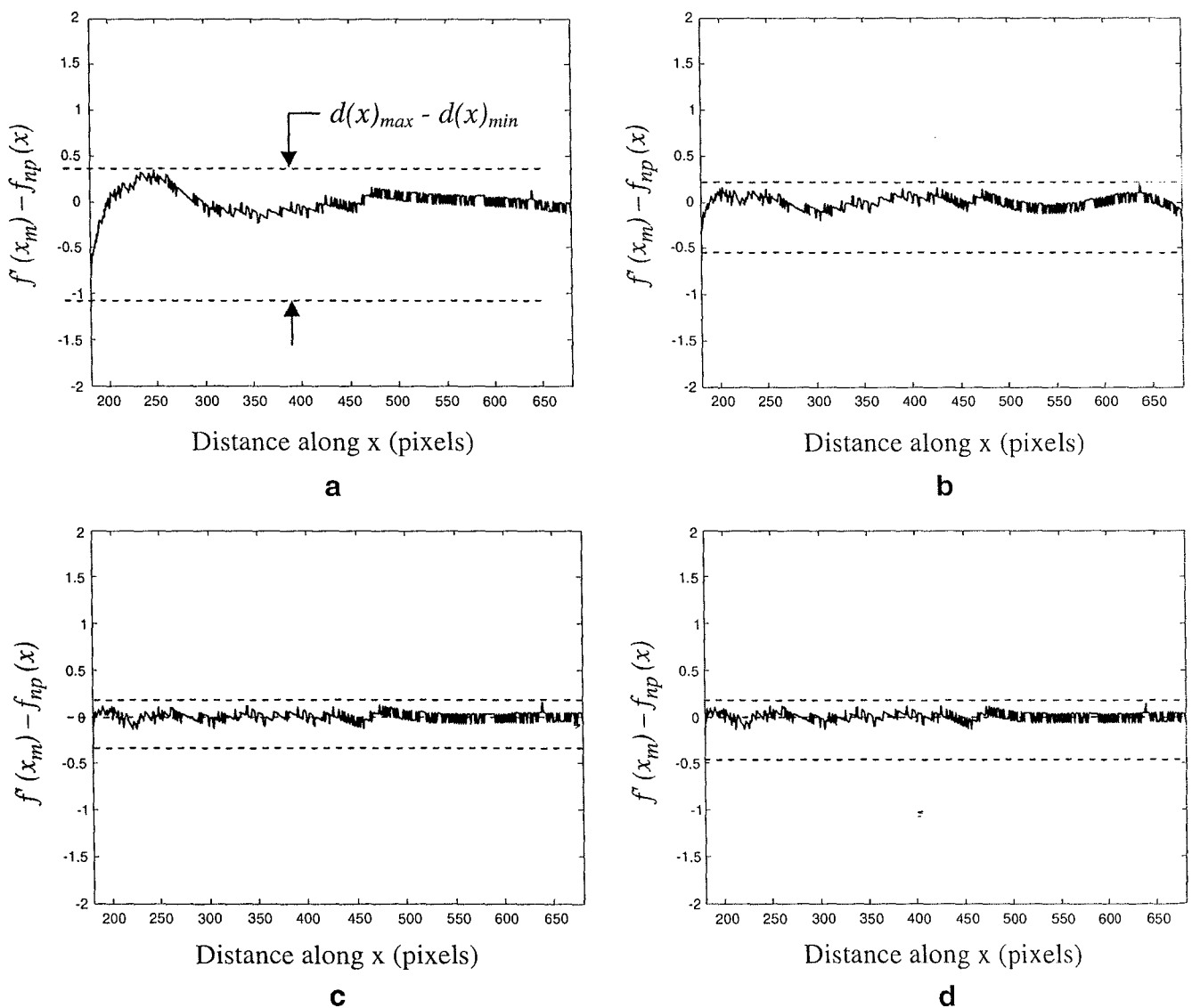


Fig. 5 Variation of $d(x)_{max} - d(x)_{min}$ with polynomial degree for unworn cutting tool: (a) $n=3$, (b) $n=5$, (c) $n=7$ and (d) $n=9$

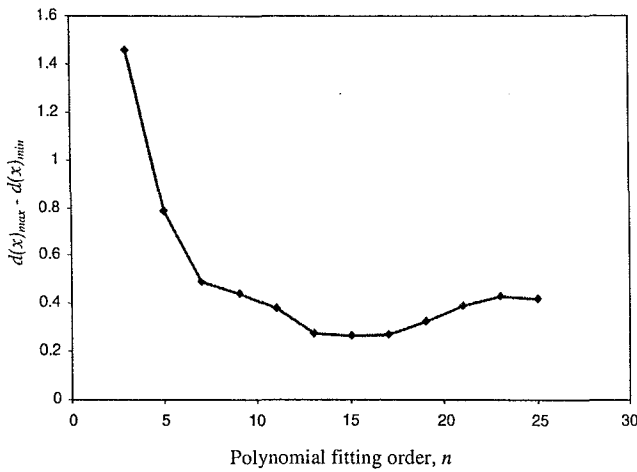


Fig. 6 Variation of $d(x)_{max} - d(x)_{min}$ with polynomial fitting order n

will reveal the location of the notch defect in the image. The notch can be detected by defining a threshold t such that when $|d(x)| > t$ a notch is considered to exist as illustrated in Fig. 1 (c). The size of the notch defect can be deduced from $|d(x)|$. The step length p was varied from $p=1$ to $p=10$ to investigate the effect of p on the capability of the proposed algorithm in detecting the presence of the notch defect.

3 Algorithm for notch wear detection

The various stage of determining of notch wear location is shown in Fig. 2 and is described as follows:

(a) Image binarization

Since the method of notch detection is based on gradient changes in a 2-D image, it was sufficient to work with binary images. The original image that exists in the gray-scale format is converted to a binary image using a simple thresholding method. This method changes all gray values

below a certain pixel threshold T to 0 and those above T to 1. The value of T can be determined from the histogram of the original grayscale image.

(b) Image rotation

The binarized image is rotated clockwise by 90° because the algorithm used to detect the gradient was written such that scanning starts at the upper left of the image and ends at the lower left. In each row, the horizontal scanning stops when a black (0) pixel is encountered and the gradient calculation will then proceed.

(c) Gradient computation

The measurement procedure, referred to as orthogonal scanning, involves repetitive horizontal scanning to determine gradient at each pixel on the tool edge (Fig. 3). The horizontal scan line starts from the point of origin [1,1] and ends at a point on lower left of the image. For simplicity, for the i -th scan line $S_L(i)$ the start point is denoted as $P_V(i)$ and the end point as $P_G(i)$ at the black pixel. The corresponding j value at the intersection is denoted as $j(i)$. When the end point $P_G(i)$ is met, the scanning is repeated at $S_L(i-p)$ and $S_L(i+p)$ and the locations $j(i-p)$ and $j(i+p)$ are recorded as j_1 and j_2 respectively. For $p=5$, the gradient at point $P_G(i)$ is given by:

$$m = \frac{j_2 - j_1}{(i + 5) - (i - 5)} = \frac{j_2 - j_1}{10} \tag{5}$$

(d) Polynomial fitting

In this stage, the gradient data is fitted with a polynomial function of degree n using the Matlab function *polyfit(x,y,n)*. The result of this function is a row vector of length $n+1$ containing the polynomial coefficients in descending powers:

$$p(x) = p_1x^n + p_2x^{n-1} + \dots + p_nx + p_n \tag{6}$$

(e) Determination of notch wear location

In order to determine the notch wear location, the polynomial fitted data was subtracted from the gradient

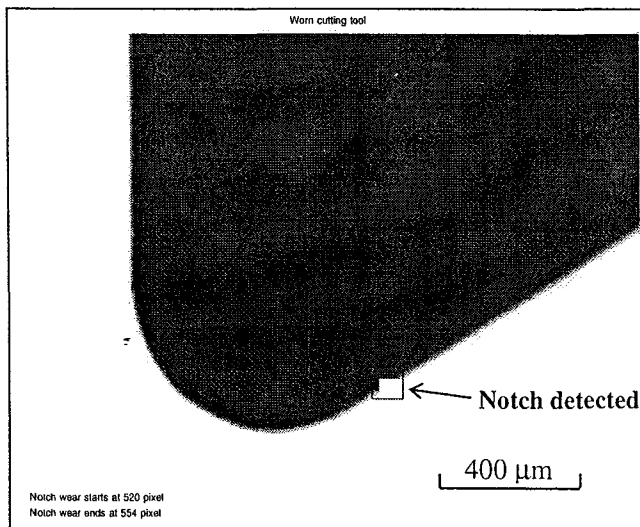


Fig. 7 Notch wear detected on cutting tool having simulated notch

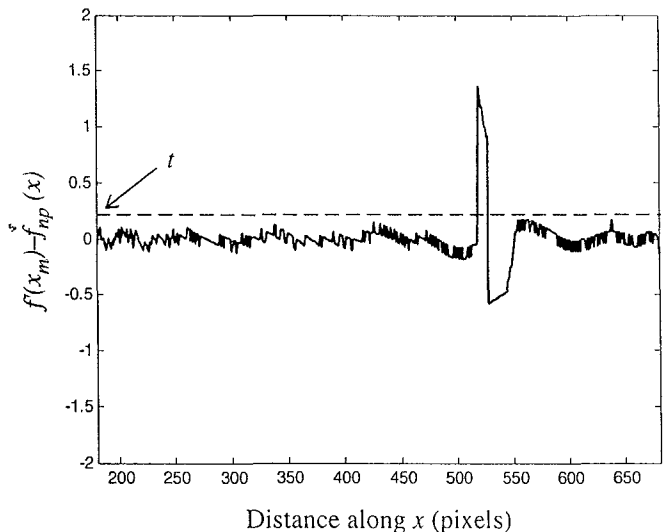
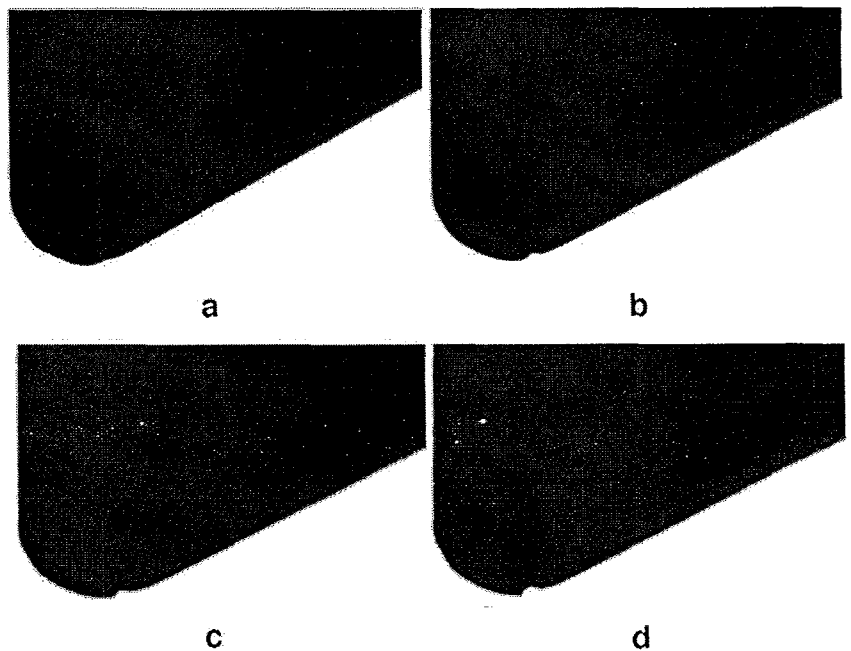


Fig. 8 Worn cutting tool with notch wear at various machining times: (a) 10 minutes, (b) 20 minutes, (c) 30 minutes and (d) 40 minutes. (Machining speed: 134 m/min, feed rate=0.25 m/min, depth of cut=0.5 mm)



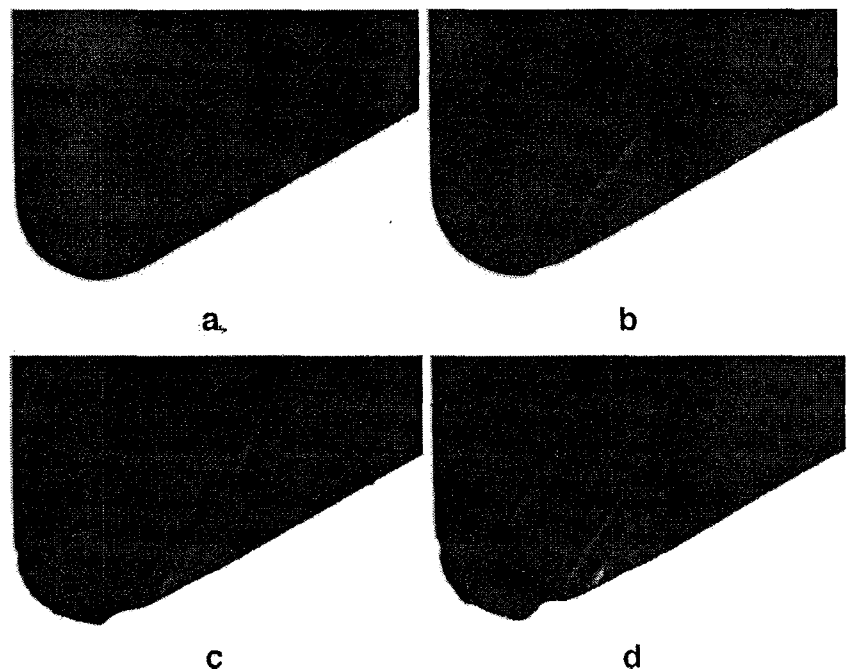
data, resulting in the difference data $d(x)$ given by Eq. (4). A threshold t is defined that determines the cut-off for deciding whether a notch exists.

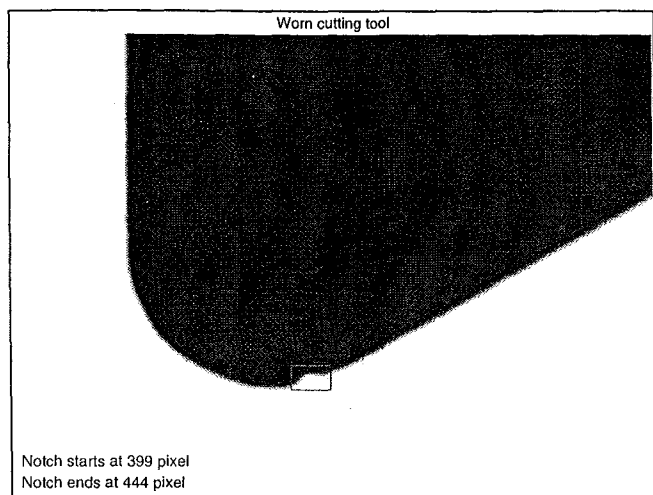
4 System configuration and methodology

A high-resolution CCD camera (JAI CV-A1, resolution 1296×1024 pixels) fitted with a 16-mm lens was used to capture images of the tool tips for different machining time.

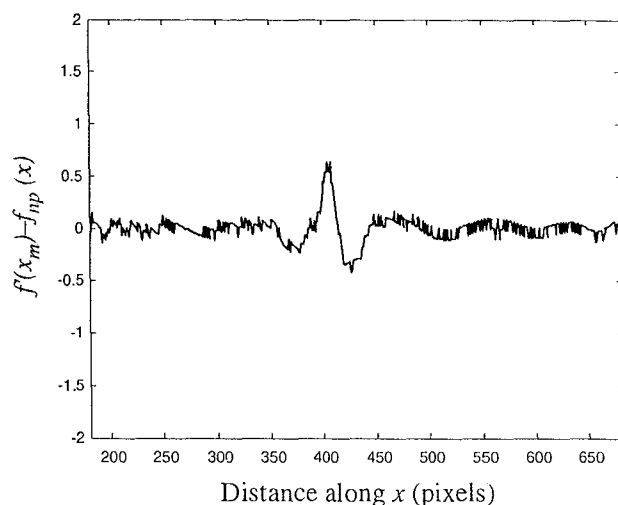
The system was mounted on a conventional lathe machine (*Pinocho S90/206*). A schematic diagram of the arrangement is shown in Fig. 4 (a) and a photograph of the setup is shown in Fig. 4 (b). Back-lighting was used to highlight the contour of the tool using a reflector. The field of view of camera is $2.3 \text{ mm} \times 2 \text{ mm}$ and the distance of camera from the cutting tool is about 60 mm. Table 1 show the various parameters used to shape the worn area. Low-carbon steels bars of diameter (D) 50 mm were used as the workpiece. The cutting tools were uncoated carbide inserts, manufactured by

Fig. 9 Worn cutting tool with notch wear at various machining times: (a) 10 minutes, (b) 20 minutes, (c) 30 minutes and (d) 40 minutes. (Machining speed: 190 m/min, feed rate=0.25 m/min, depth of cut=0.5 mm)

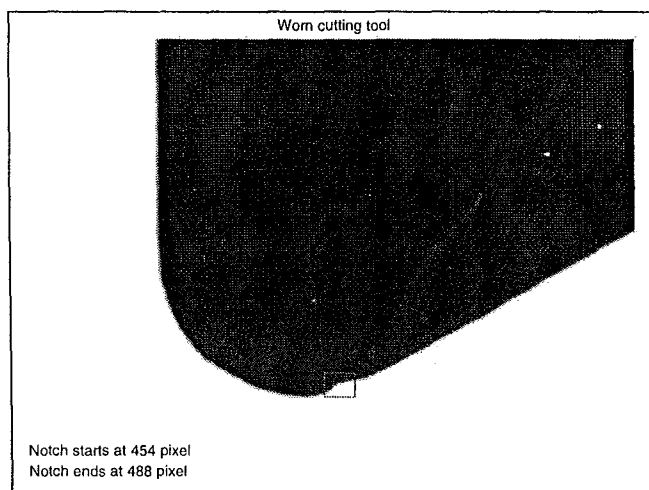




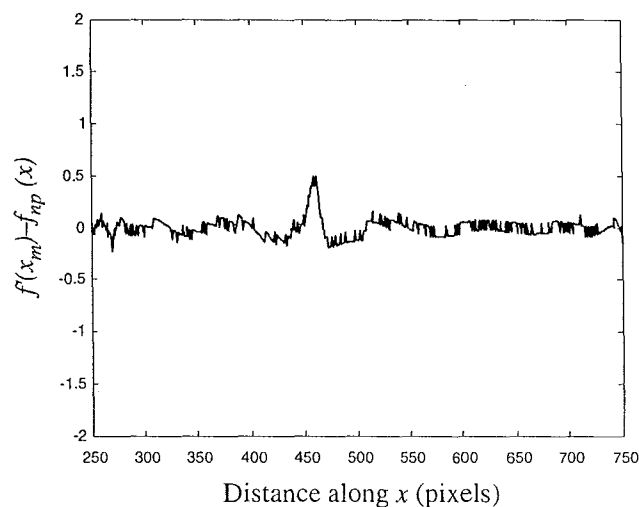
a



b



c



d

Fig. 10 (a) Worn tool with notch wear detected for cutting speed 134 m/min, (b) variation of $d(x)$ with distance along x for image in (a), (c) worn tool with notch wear detected for cutting speed 190 m/min, (d) variation of $d(x)$ with distance along x for figure image in (a)

Sandvik Co. Ltd., Sweden. The cutting speed was initially fixed at 134 m/min, and four different machining times at 10 minutes intervals were used to determine the rate of tool wear. The experiment was repeated by changing the cutting speed to 190 m/min, while keeping the other parameters constant.

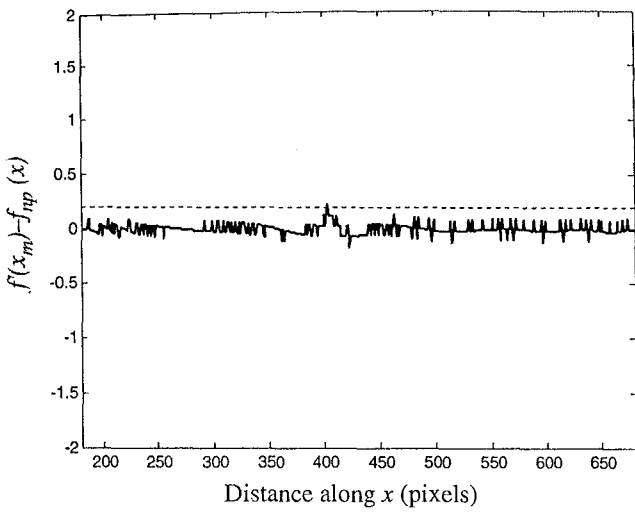
5 Results and discussion

The results of this study are presented in three sections. In Section 5.1, results of determination of the best polynomial coefficient to fit the data using simulated images are discussed. In Section 5.2 the results of application to real images is presented. In Section 5.3, the effect of changing

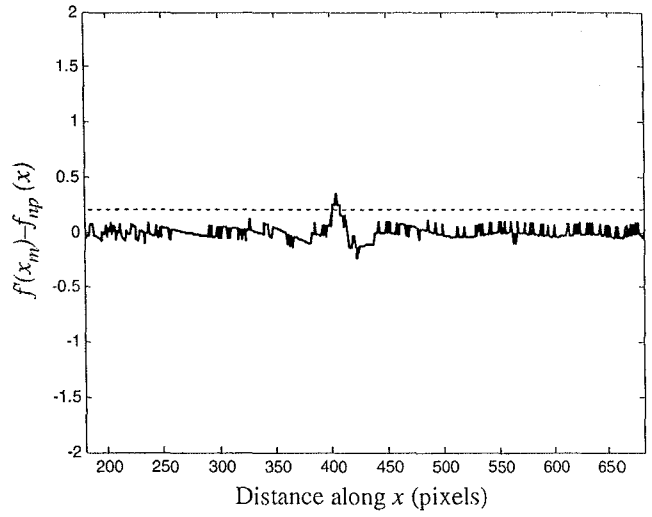
the step length p on the ability of the proposed technique to detect the notch wear is discussed.

5.1 Determination of the best polynomial degree

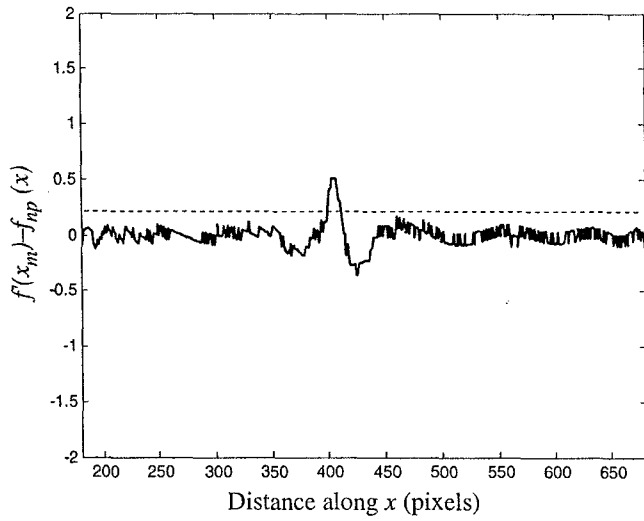
The performance of the proposed method of detecting notch wear is highly dependent upon the degree of the polynomial $p(x)$ used to fit the gradient data. Thus, it is necessary to investigate the effect of polynomial degree n on the accuracy of the technique. A trial-and-error approach was adopted whereby a program written in *Matlab* was used to change the degree n to determine the best value that can reveal the notch defect. In order to do this, the difference $d(x)$ for an unworn tool was determined for different polynomial degrees of fitting. The degree n was changed



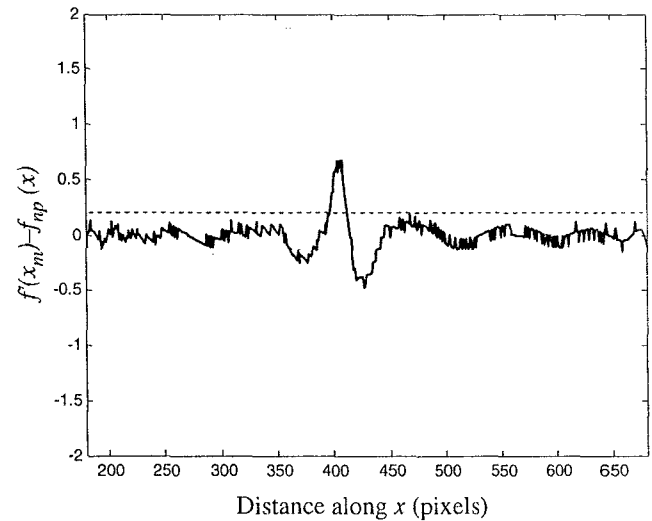
a $p = 1$



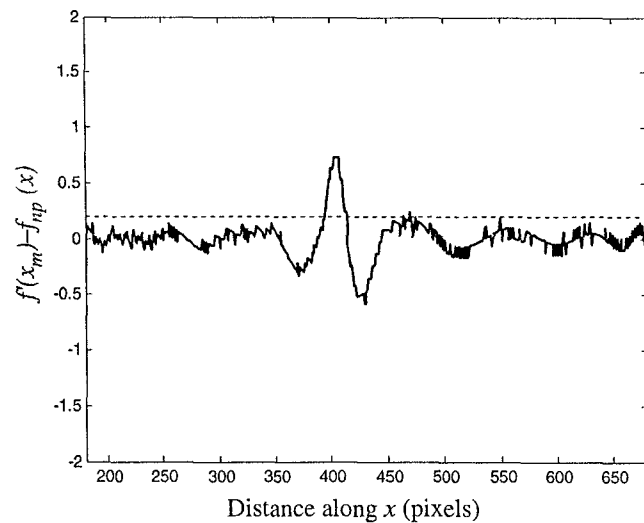
b $p = 2$



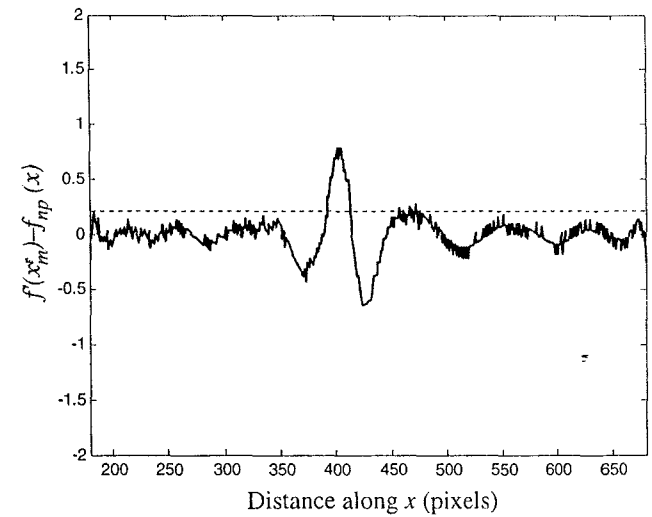
c $p = 4$



d $p = 6$



e $p = 8$



f $p = 10$

Fig. 11 Effect of step length p (pixels) on detection of notch (machining duration=20 minutes)

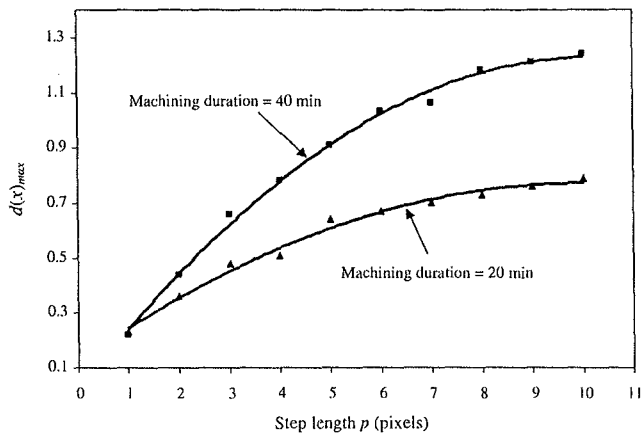


Fig. 12 Variation of $d(x)_{max}$ with step length p

from 3 to 25 in odd increments and the difference between the maximum and minimum values of $d(x)$, i.e., $d(x)_{max} - d(x)_{min}$ was evaluated for each case. Figures 5 (a)-(d) illustrate how $d(x)$ varies with distance along x -direction for various values of n . Figure 6 shows the variation of $d(x)_{max} - d(x)_{min}$ with polynomial degree for an unworn cutting tool. The polynomial of degree $n=15$ was found to give the smallest value of $d(x)_{max} - d(x)_{min}$. Thus, this value was used when analyzing worn tools to detect the presence of notch wear. Since $d(x)_{max}=0.137$ when $n=15$ for the unworn tool, the threshold for detecting notch wear was set above this value, i.e., $t=0.2$. This threshold can be adjusted depending on the minimum size of notch to be detected.

In order to determine the smallest size of notch wear that can be detected using the set threshold, notches of various sizes were generated on an unworn cutting tool using the software tools in *Matlab*. Figure 7 shows an example of the notch generated and the results of detection using the algorithm developed. The actual area of the notch can be determined by subtracting the images of worn and unworn cutting tools. The smallest notch that can be detected using $t=0.2$ was found to be five pixels. Using a scaling factor of $1.88 \mu\text{m} \times 2.00 \mu\text{m}$ (determined by calibration using pin gages), we found that the smallest notch area corresponds to $1.88 \times 10^{-5} \text{mm}^2$. The simulation study was also repeated by moving the notch to different locations and introducing more than one notch. In all these cases, the notch defects were detected successfully.

5.2 Application to real images

The cutting tools were captured before machining to get the initial image of tool tip. The cutting speed was initially fixed at 134 m/min and other machining conditions are shown in Table 1. Images of worn cutting tool tips were captured during different time intervals. Figures 8 (a)-(d) show images of the tool at different machining time where

the growth of notch is clearly visible after 20 minutes of machining. Figures 9 (a)-(d) show another set of images captured under a different cutting speed (190 m/min) where as in the previous case the notch becomes visible after 20 minutes. The notch wear location was automatically determined using the algorithm developed in this study. Figure 10 (a) shows the results obtained for a cutting tool after 40 minutes of machining where the notch has been successfully detected using $t=0.2$ (cutting speed 134 m/min). Similarly, Fig. 10 (c) show the result of notch detection for the repeated study after 20 minutes of machining (cutting speed 190 m/min). The location of the notch measured in the horizontal direction from the left of the image is displayed on the lower left corner of both images. From Figs. 10 (b) and (d) the effect of the notch on the difference $d(x) = f'(x_m) - f_{np}(x)$ is clearly visible. An abrupt increase in the value of $d(x)$ can be observed at the notch. The detection was repeated for other machining durations and in all cases the presence of the notch could be detected. The results for both cutting speeds show that the notch wear can be detected successfully using the proposed gradient approach.

5.3 Effect of changing step length p

The step length was varied from $p=1$ to $p=10$ pixels to study its effect on the ability of the proposed algorithm for detecting the notch defect. Images of the cutting tool insert machined for durations of 20 and 40 minutes (Figs. 8 (b) and (d)) were used in this study. Figures 11 (a)-(f) show the variation of the difference $f'(x_m) - f_{np}(x)$ along the x -direction for machining duration of 20 minutes. For the same notch size it was found that the maximum difference $d(x)_{max}$ increased with p approximately as a second degree polynomial function (Fig. 12). Similar trends were observed for the insert machined for 40 minutes (larger notch wear). From Figs. 11 (a)-(f) a general increase in the waviness of the difference plot can be seen as p increases. This is due to the increase in error when a larger step size is used in the gradient calculation. For the smallest step size of $p=1$ pixel the presence of notch can still be detected because the maximum difference $d(x)_{max}$ exceeds the threshold of $t=0.2$. For a larger step size, e.g., $p>10$ pixels, the region where the presence of notch is searched has to be made smaller, thus missing notches outside this region. Therefore, a value of p between two to ten pixels is adequate for the detection of notch defects.

6 Conclusion

The gradient detection algorithm with polynomial fitting proposed in the work is able to detect the location of

microscopic notch wear defects accurately from a single 2-D image of cutting tools. A camera mounted directly on the lathe machine enables image of the tool to be captured in-cycle (intermittently during machining) and analyzed without the need to dismantle the tool from the machine. Since previous researchers have shown that notch wear has a direct effect on the surface roughness of the workpiece, the proposed technique can be used to detect problems early in the machining and prevent poor surface quality in products. The use of a single image overcomes the need for positioning the camera accurately above the cutting tool.

Acknowledgement The authors would like to thank Universiti Sains Malaysia for the offer of the short-term grant that enabled this study to be carried out and the reviewers for their valuable comments and criticisms on this work.

References

1. Kurada S, Bradley C (1997) A review of machine vision sensors for tool condition monitoring. *Computer in Industry* 34:55–72
2. Kurada S, Bradley C (1997) A machine vision system for tool wear assessment. *Tribol Int* 30:295–304
3. International Standard (1993) Tool-life testing with single-point turning tools: ISO 3685 2nd Edition, Switzerland
4. Wang WH, Hong GS, Wong YS (2006) Flank wear measurement by threshold independent method with sub-pixel accuracy. *Int J Mach Tools Manuf* 46:199–207
5. Wang WH, Wong YS, Hong GS (2005) Flank wear measurement by successive image analysis. *Computer in Industry* 56:816–830
6. Pfeifer T, Wieggers L (2000) Reliable tool wear monitoring by optimized image and illumination control in machine vision. *Measurement* 28:209–218
7. Sortino M (2003) Application of statistical filtering for optical detection of tool wear. *Int J Mach Tools Manuf* 43:493–497
8. Jeon JU, Kim SW (1988) Optical flank wear monitoring of cutting tools by image processing. *Wear* 127:207–217
9. Wang WH, Wong YS, Hong GS (2006) 3D measurement of crater wear by phase shifting method. *Wear* 261:164–171
10. Jurkovic J, Korosec M, Kopac J (2005) New approach in tool wear measuring technique using CCD vision system. *Int J Mach Tools Manuf* 45(2005):1023–1030
11. Ghani AK, Choudhury IA, Husni (2002) Study of tool life, surface roughness and vibration in machining nodular cast iron with ceramic tool. *J Mater Process Technol* 127:17–22
12. Pavel R, Marinescu J, Deis M, Pillar J (2005) Effect of tool wear on surface finish for a case of continuous and interrupted hard turning. *J Mater Process Technol* 170(3):341–349
13. Kwon Y, Fischer GW (2003) A novel approach to quantifying tool wear and tool life measurements for optimal tool management. *Int J Mach Tools Manuf* 43:359–368



MINISTRY OF SCIENCE,
TECHNOLOGY & INNOVATION

ITEX
MALAYSIA

Invention - Innovation
Industrial Design - Technology



Certificate of Award

This is to certify that

**ASSOC PROF DR MANI MARAN RATNAM, HAMIDREZA
H SHAHABI**

has been awarded the

ITEX BRONZE MEDAL

for the invention

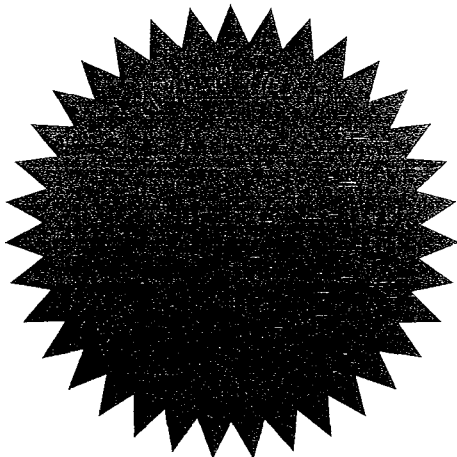
**TOOLMON: TOOL WEAR MONITORING AND
MEASUREMENT SYSTEM FOR LATHE MACHINES**

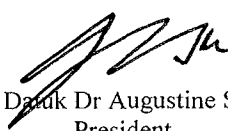
at the

**18th International Invention, Innovation & Technology Exhibition
ITEX 2007
Kuala Lumpur, Malaysia**

held from

18th – 20th May 2007




Tan Sri Datuk Dr Augustine S. H. Ong
President
Malaysian Invention and Design Society